



1 **Recent updates on the Copernicus Marine Service global**
2 **ocean monitoring and forecasting real-time 1/12° high**
3 **resolution system**

4
5 Jean-Michel Lellouche¹, Eric Greiner², Olivier Le Galloudec¹, Gilles Garric¹, Charly
6 Regnier¹, Marie Drevillon¹, Mounir Benkiran¹, Charles-Emmanuel Testut¹, Romain
7 Bourdalle-Badie¹, Florent Gasparin¹, Olga Hernandez¹, Bruno Levier¹, Yann Drillet¹,
8 Elisabeth Remy¹, Pierre-Yves Le Traon^{1,3}

9
10 ¹ Mercator Ocean, Ramonville Saint Agne, France

11 ² Collecte Localisation Satellites, Ramonville Saint Agne, France

12 ³ IFREMER, 29280, Plouzané, France

13
14 *Correspondence to:* Jean-Michel Lellouche (jlellouche@mercator-ocean.fr)

15
16 **Abstract**

17 Since October 19, 2016, and in the framework of Copernicus Marine Environment
18 Monitoring Service (CMEMS), Mercator Ocean delivers in real-time daily services (weekly
19 analyses and daily 10-day forecasts) with a new global 1/12° high resolution (eddy-resolving)
20 monitoring and forecasting system. The model component is the NEMO platform driven at
21 the surface by the IFS ECMWF atmospheric analyses and forecasts. Observations are
22 assimilated by means of a reduced-order Kalman filter with a 3D multivariate modal
23 decomposition of the forecast error. Along track altimeter data, satellite sea surface
24 temperature, sea ice concentration and in situ temperature and salinity vertical profiles are
25 jointly assimilated to estimate the initial conditions for numerical ocean forecasting. A 3D-
26 VAR scheme provides a correction for the slowly-evolving large-scale biases in temperature
27 and salinity.

28 This paper describes the recent updates applied to the system and discusses the importance of
29 fine tuning of an ocean monitoring and forecasting system. It details more particularly the
30 impact of the initialization, the correction of precipitation, the assimilation of climatological
31 temperature and salinity in the deep ocean, the construction of the forecast error covariance



1 and the adaptive tuning of observations error on increasing the realism of the analysis and
2 forecasts.

3 The scientific assessment of the ocean estimations are illustrated with diagnostics over some
4 particular years, assorted with time series over the time period 2007-2016. The overall impact
5 of the integration of all updates on the products quality is also discussed, highlighting a gain
6 in performance and reliability of the current global monitoring and forecasting system
7 compared to its previous version.

8

9 **1 Introduction**

10 Mercator Ocean monitoring and forecasting systems have been routinely operated in real-time
11 since early 2001 and have been regularly upgraded by increasing complexity, expanding the
12 geographical coverage from regional to global and improving models and assimilation
13 schemes (Brasseur et al., 2006; Lellouche et al., 2013).

14 After having successfully coordinated the European MyOcean and MyOcean2 projects
15 (<http://www.myocean.eu>), Mercator Ocean was officially entrusted by the European
16 Commission on November, 11, 2014 to implement and operate the Copernicus Marine
17 Environment Monitoring Service (CMEMS), as part of the European Earth observation
18 program Copernicus (<http://marine.copernicus.eu>). Since January 2009, Mercator Ocean,
19 which had primary responsibility for the global ocean forecasts of the MyOcean project,
20 developed several versions of its monitoring and forecasting systems for the various
21 milestones (from V0 to V4) of the MyOcean project, and more recently, for milestones V1,
22 V2 and V3 of the CMEMS (Fig. 1). The main differences and links between the various
23 versions of the Mercator Ocean systems in the framework of past MyOcean project and
24 current CMEMS are summarized in Table 1 and Table 2 for Intermediate Resolution $\frac{1}{4}^\circ$ Global
25 configurations (hereafter IRG) and High Resolution $1/12^\circ$ Global configurations (hereafter
26 HRG) systems respectively.

27 These systems are intensively used in four main areas of application: maritime safety, marine
28 resources management, coastal and marine environment, and weather, climate and seasonal
29 forecasting (<http://marine.copernicus.eu/markets/use-cases>). As described in Lellouche et al.
30 (2013), the evaluation of such systems includes routine verification against assimilated and
31 independent in situ and satellite observations, as well as a careful check of many physical
32 processes (e.g. mixed layer depth evaluation as shown in Drillet et al. (2014)). Scientific



1 studies brought precious additional evaluation feedbacks (Juza et al., 2015; Smith et al., 2016;
2 Estournel et al., 2016). Finally, several studies showed the added value of surface currents
3 analyses provided by these systems for drift applications (Scott et al., 2012; Drevillon et al.,
4 2013).

5 Since May 2015, Mercator Ocean opened the CMEMS and has been in charge of the global
6 high resolution ocean analyses and forecasts. In this context, R&D activities have been
7 conducted these last years to improve the real-time $1/12^\circ$ high resolution (eddy-resolving)
8 global analysis and forecasting system. Since October 19, 2016, Mercator Ocean delivers in
9 real-time daily services (weekly analyses and daily 10-day forecasts) with a new global $1/12^\circ$
10 system PSY4V3R1 (hereafter PSY4V3, and corresponding to HRG_V2V3 in Fig. 1). Note
11 that PSY4V3 will be the system for the CMEMS V4 milestone. In this system, the ocean/sea
12 ice model and the assimilation scheme benefit of the following main updates: atmospheric
13 forcing fields are corrected at large-scale with satellite data; freshwater runoff from ice sheets
14 melting is added to river runoffs; a time varying global average steric effect is added to the
15 model sea level; the last version of GOCE geoid observations are taken into account in the
16 Mean Dynamic Topography used for Sea Level Anomalies assimilation; adaptive tuning is
17 used on some of the observational errors; a dynamic height criteria is added to the Quality
18 Control of the assimilated temperature and salinity vertical profiles; satellite sea ice
19 concentrations are assimilated; climatological temperature and salinity in the deep ocean are
20 assimilated below 2000 m to prevent drifts in those very sparsely observed depths.

21 The impact of all these updates can be evaluated separately, thanks to an incremental
22 implementation, taking advantage of Mercator Ocean's specific hierarchy of system
23 configurations running with identical set up. To this aim, short simulations (from one year to a
24 few years) were performed by adding from one simulation to another one upgrade at a time,
25 using the IRG configuration or some high resolution $1/12^\circ$ regional configuration.

26 Moreover, in the development phase of an operational system, it was decided to
27 systematically perform three twin numerical simulations over a given time period,
28 maintaining the same ocean model tunings but varying the complexity and the level of data
29 assimilation. Inter-comparisons between the three simulations were then conducted in order to
30 better analyze and to try to quantify the impact of some component of the assimilation system.
31 These three versions of system have also been used to quantify the impact of some updates.

32 In a previous paper (Lellouche et al., 2013), the main results of the scientific evaluation of
33 MyOcean global monitoring and forecasting systems at Mercator Ocean showed how



1 refinements or adjustments to the system impacted the quality of ocean analyses and
2 forecasts. The primary objective of this paper is to describe the recent updates applied to the
3 system PSY4V3. The updates showing the highest impact on the products quality are
4 separately illustrated and discussed, with a particular focus on the initialization, the correction
5 of precipitation, the assimilation of climatological temperature and salinity in the deep ocean,
6 the construction of the forecast error covariance and the adaptive tuning of observations error.
7 Another objective of this paper is to present a first level evaluation of the system. The purpose
8 here is not to perform an exhaustive validation but only to check the global behavior of the
9 system compared to assimilated quantities or independent observations. Thus, an assessment
10 of the hindcasts (2007-2016) quality is conducted and improvements with respect to the
11 previous system are highlighted in order to show the level of performance and the reliability
12 of the system PSY4V3. A complementary study aimed at demonstrating the scientific value of
13 PSY4V3 for resolving oceanic variability at regional and global scale (Gasparin et al., 2018 -
14 Submitted in Journal of Marine Systems). Lastly, several scientific studies have investigated
15 local ocean processes by comparing the PSY4V3 system with independent observations
16 campaigns (Koenig et al., 2017; Artana et al., 2018 - Submitted in Journal of Geophysical
17 Research - Oceans). This reinforces the system PSY4V3 evaluation effort.

18 This paper is organized as follows. The main characteristics of the system PSY4V3 and
19 details concerning the updates are described in Sect. 2. The impact of the most sensitive
20 upgrades is shown in Sect. 3. Results of the scientific evaluation, including some comparisons
21 with independent observations, are given in Sect. 4. Section 5 contains a summary of the
22 scientific assessment, as well as a discussion of the future improvements for the next version
23 of the global high resolution system.

24

25 **2 Description of the current global high resolution monitoring and** 26 **forecasting system PSY4V3**

27 This section contains the main characteristics of the CMEMS system PSY4V3 and details the
28 last updates to the system compared to the previous system PSY4V2R2 (hereafter PSY4V2,
29 and corresponding to HRG_V3V4_V1V2 in Fig. 1). A detailed description of the main
30 updates is provided in Sect. 3.



1 **2.1 Physical model and latest updates**

2 The system PSY4V3 uses version 3.1 of the NEMO ocean model (Madec et al., 2008). This
3 NEMO version is available since a few years and has been already used in the previous
4 system PSY4V2. However, all the schemes and the parameterizations used in this version are
5 still available in the current NEMO 3.6 stable version that is now the standard version of the
6 code. The physical configuration is based on the tripolar ORCA12 grid type (Madec and
7 Imbard, 1996) with a horizontal resolution of 9 km at the equator, 7 km at Cape Hatteras
8 (mid-latitudes) and 2 km toward the Ross and Weddell seas. The 50-level vertical
9 discretization retained for this system has a decreasing resolution from 1m at the surface to
10 450 m at the bottom, and 22 levels within the upper 100 m. A “partial cells” parameterization
11 (Adcroft et al., 1997) is chosen for a better representation of the topographic floor (Barnier et
12 al., 2006) and the momentum advection term is computed with the energy and enstrophy
13 conserving scheme proposed by Arakawa and Lamb (1981). The advection of the tracers
14 (temperature and salinity) is computed with a total variance diminishing (TVD) advection
15 scheme (Levy et al., 2001; Cravatte et al., 2007). We use a free surface formulation. External
16 gravity waves are filtered out using the Roullet and Madec (2000) approach. A laplacian
17 lateral isopycnal diffusion on tracers ($100 \text{ m}^2 \text{ s}^{-1}$) and a horizontal biharmonic viscosity for
18 momentum ($-2e10 \text{ m}^4 \text{ s}^{-1}$) are used. In addition, the vertical mixing is parameterized according
19 to a turbulent closure model (order 1.5) adapted by Blanke and Delecluse (1993), the lateral
20 friction condition is a partial-slip condition with a regionalization of a no-slip condition (over
21 the Mediterranean Sea) and the Elastic-Viscous-Plastic rheology formulation for the LIM2 ice
22 model (Fichefet and Maqueda, 1997) has been activated (Hunke and Dukowicz, 1997).
23 Instead of being constant, the depth of light extinction is separated in Red-Green-Blue bands
24 depending on the chlorophyll data distribution from mean monthly SeaWIFS climatology
25 (Lengaigne et al., 2007). The bathymetry used in the system is a combination of interpolated
26 ETOPO1 (Amante and Eakins, 2009) and GEBCO8 (Becker et al., 2009) databases. ETOPO1
27 datasets are used in regions deeper than 300 m and GEBCO8 is used in regions shallower than
28 200 m with a linear interpolation in the 200 - 300 m layer. Internal-tide driven mixing is
29 parameterized following Koch-Larrouy et al. (2008) for tidal mixing in the Indonesian Seas,
30 as the system doesn't represent explicitly the tides. The atmospheric fields forcing the ocean
31 model are taken from the ECMWF (European Centre for Medium-Range Weather Forecasts)
32 IFS (Integrated Forecast System). A 3 h sampling is used to reproduce the diurnal cycle.
33 Momentum and heat turbulent surface fluxes are computed from the Large and Yeager (2009)



1 bulk formulae using the following set of atmospheric variables: surface air temperature and
2 surface humidity at a height of 2 m, mean sea level pressure and wind at a height of 10 m.
3 Downward longwave and shortwave radiative fluxes and rainfall (solid + liquid) fluxes are
4 also used in the surface heat and freshwater budgets. Compared to the previous HRG system
5 PSY4V2, the following updates were done on the model part (see Table 2):

- 6 - The bathymetry used in the system benefited from a specific correction in the Indonesian
7 Sea inherited from the INDESO system (Tranchant et al., 2016).
- 8 - In order to solve numerical problems induced by the use of z-coordinates on the vertical
9 (Willebrand et al., 2001), a relaxation toward the World Ocean Atlas 2013 (version 2)
10 2005-2012 time period (hereafter WOA13v2,
11 https://data.nodc.noaa.gov/woa/WOA13/DOC/woa13v2_changes.pdf) temperature
12 (Locarnini et al., 2013) and salinity (Zweng et al., 2013) climatology has been added at
13 Gibraltar and Bab-el-Mandeb straits. For Gibraltar (respectively Bab-el-Mandeb), the
14 relaxation area is centered at 8° W, 35° N (respectively 46° E, 12° N). At the center the
15 relaxation time is 10 days (respectively 50 days). This time is increased up to infinity 4°
16 (respectively 5°) away from the center. The relaxation is not constant over the vertical. It
17 is only applied below 500 m and it is increased linearly between 500 to 700 m. Between
18 700 m and the bottom of the ocean the coefficient value is unchanged.
- 19 - Surface wind stress computation should in principle consider wind speed relative to the
20 surface ocean currents (Bidlot, 2012; Renault et al., 2016). However, this statement
21 applies to a fully coupled ocean/atmosphere system, which is not the case for the present
22 system PSY4V3. Based on sensitivity experiments, we pragmatically consider only 50 %
23 of the surface model currents in the wind stress computation.
- 24 - The monthly runoff climatology is built with data on coastal runoffs and 100 major rivers
25 from the Dai et al. (2009) database (instead of Dai and Trenberth (2002) for the system
26 PSY4V2). This database uses new data, mostly from recent years, streamflow simulated
27 by the Community Land Model version 3 (CLM3) to fill the gaps, in all lands areas except
28 Antarctica and Greenland. In addition, we built mean seasonal freshwater fluxes
29 representing Greenland and Antarctica ice sheets and glaciers runoff melting. For this
30 purpose we have distributed IPCC-AR13 (Church et al., 2013) mean values, 1.51 mm yr⁻¹
31 for Greenland and 6.65 mm yr⁻¹ for Antarctica, onto a domain varying seasonally and
32 defined by the Altiberg icebergs database project (Tournadre et al., 2013). Domain
33 covered by giant icebergs from Silva et al. (2006) completes southern most areas not
34 covered by Altiberg data. One third of these quantities is applied off shore and two third



- 1 along Greenland and Antarctic coastlines. We also used negative gridded GRACE
2 anomalies (Bruinsma et al., 2010) to distribute spatially these runoffs along coastlines.
- 3 - As the Boussinesq approximation is applied to the model equations, conserving the ocean
4 volume and varying its mass, the simulations do not properly directly represent the global
5 mean steric effect on the sea level (Greatbatch, 1994). For improved consistency with
6 assimilated satellite observations of sea level anomalies, which are unfiltered from the
7 global mean steric component, a time-evolving global average steric effect is added to the
8 sea level in the simulation. This global average steric effect has been computed as the
9 difference between two successive daily global mean dynamic heights (vertical
10 integration, from the surface to the bottom, of the specific volume anomaly).
- 11 - Due to large known biases in precipitations, a satellite-based large-scale correction of
12 precipitations has been performed, except at high latitudes (poleward of 65° N and 60° S).
13 This is detailed in Sect. 3.
- 14 - In order to avoid mean sea-surface-height drift due to the large uncertainties in the water
15 budget closure, the following treatments were applied:
- 16 o The surface freshwater global budget is set to an imposed seasonal cycle (Chen et
17 al., 2005). Only spatial departures from the mean global budget are kept from the
18 forcing.
 - 19 o A trend of 2.2 mm yr⁻¹ has been added to the surface mass budget in order to
20 represent the recent estimate of the global mass addition to the ocean (from
21 glaciers, land water storage changes, Greenland and Antarctica ice sheets mass
22 loss) (Chambers et al., 2017). This term is implemented as a surface freshwater
23 flux in the open ocean domain infested by observed icebergs.

24 **2.2 Data assimilation and latest updates**

25 The data are assimilated by means of a reduced-order Kalman filter derived from a SEEK
26 filter (Brasseur and Verron, 2006), with a 3D multivariate modal decomposition of the
27 forecast error and a 7-day assimilation cycle. It includes an adaptive-error estimate and a
28 localization algorithm. This data assimilation system is called SAM (Système d'Assimilation
29 Mercator). The forecast error covariance is based on the statistics of a collection of 3D ocean
30 state anomalies, typically a few hundreds (250 anomalies for PSY4V3). The anomalies are
31 computed from a long numerical experiment (9 years for PSY4V3) with respect to a running
32 mean in order to estimate the 7-day scale error on the ocean state at a given period of the year.



1 A Hanning low-pass filter is used to create the running mean with a cut-off frequency equal to
2 $1/24 \text{ days}^{-1}$. Altimeter data, in situ temperature and salinity vertical profiles, and satellite sea
3 surface temperature and sea ice concentration are jointly assimilated to estimate the initial
4 conditions for numerical ocean forecasting. In addition, a 3D-VAR scheme provides a
5 correction for the slowly-evolving large-scale biases in temperature and salinity (Lellouche et
6 al., 2013).

7 Compared to the previous HRG system PSY4V2, the following updates were done on the data
8 assimilation part (see Table 2):

9 - CMEMS satellite sea ice concentration OSI SAF
10 ([http://marine.copernicus.eu/documents/QUID/CMEMS-OSI-QUID-011-001to007-](http://marine.copernicus.eu/documents/QUID/CMEMS-OSI-QUID-011-001to007-009to012.pdf)

11 [009to012.pdf](http://marine.copernicus.eu/documents/QUID/CMEMS-OSI-QUID-011-001to007-009to012.pdf)) is a new observation assimilated in the system PSY4V3. For this, a separate
12 monovariate/monodata analysis is carried out for the ice variables, in parallel to that for
13 the ocean. The two analyses are completely independent.

14 - CMEMS OSTIA SST (delayed time:
15 <http://marine.copernicus.eu/documents/QUID/CMEMS-OSI-QUID-010-011.pdf>, then

16 near real time: [http://marine.copernicus.eu/documents/QUID/CMEMS-OSI-QUID-010-](http://marine.copernicus.eu/documents/QUID/CMEMS-OSI-QUID-010-001.pdf)
17 [001.pdf](http://marine.copernicus.eu/documents/QUID/CMEMS-OSI-QUID-010-001.pdf)) is assimilated in the system PSY4V3, instead of near real time AVHRR SST
18 from NOAA in PSY4V2. A particular attention has been devoted to the computation of
19 the model equivalent. As OSTIA provides the foundation SST (considered nominally at
20 10 m depth), the SST model equivalent is performed by calculating the night-time average
21 of the first level of the model temperature.

22 - In addition to the quality control based on temperature and salinity innovation statistics
23 (detection of spikes, large biases), already present in the previous system, a second quality
24 control has been developed and is based on dynamic height innovation statistics (detection
25 of small vertically constant biases). This is detailed in Sect. 2.3.

26 - A new hybrid MDT, based on the “CNES-CLS13” MDT (Rio et al., 2014) with
27 adjustments made using the Mercator GLORYS2V3 (GLobal Ocean ReanalYsis and
28 Simulation – stream 2 – version 3) reanalysis and with an improved Post Glacial Rebound
29 (also called Glacial Isostatic Adjustment), has been used. This new hybrid MDT also takes
30 into account the last version of the GOCE geoid. This replaces the previous hybrid MDT
31 used in the previous system PSY4V2, which was based on the “CNES-CLS09” MDT
32 derived from observations (Rio et al., 2011). The new hybrid MDT significantly reduces
33 (not shown) sea level bias (more than 5 cm in some areas) and consequently temperature



- 1 and salinity in regions where the topography makes difficult the mean sea surface
2 estimation (e.g. Indonesia, Red Sea and Mediterranean Sea).
- 3 - A consistent along track SLA dataset
4 (<http://marine.copernicus.eu/documents/QUID/CMEMS-SL-QUID-008-032-051.pdf>),
5 with a 20-year altimeter reference period, is assimilated all along the simulation
6 performed with the system PSY4V3.
- 7 - The CORA 4.1 CMEMS in situ database (Szekely et al., 2016;
8 <http://marine.copernicus.eu/documents/QUID/CMEMS-INS-QUID-013-001b.pdf>) has
9 been assimilated for the 2006-2013 period. In addition to Argo and other in situ data sets,
10 this database includes temperature and salinity vertical profiles from sea mammal
11 (elephant seals) database (Roquet et al., 2011) to compensate for the lack of such data at
12 high latitudes. From 2014 to present, the near-real time CMEMS product
13 (<http://marine.copernicus.eu/documents/QUID/CMEMS-INS-QUID-013-030-036.pdf>) is
14 assimilated.
- 15 - As the prescription of observation errors in the assimilation systems is not sufficiently
16 accurate, adaptive tuning of observation errors for the SLA and SST has been
17 implemented. The method has been adapted from diagnostics proposed by Desroziers et
18 al. (2005) and is detailed in Sect. 3.
- 19 - New 3D observation errors files for the assimilation of in situ temperature and salinity
20 data have been re-computed from the MyOcean IGR system PSY3V3R3 (corresponding
21 to IRG_V3V4 in Fig. 1) using an offline version of the adaptive tuning method mentioned
22 above.
- 23 - A weak constraint towards the WOA13v2 climatology on temperature and salinity in the
24 deep ocean (below 2000 m) has been included in the two components (3D-VAR and
25 SEEK filter) of the assimilation scheme to prevent drifts in temperature and salinity and as
26 a consequence to obtain a better representation of the sea level trend at global scale in the
27 system. The method consists in assimilating vertical climatological profiles of temperature
28 and salinity at large scale and below 2000 m in regions drifting away from the
29 climatological values, using a non-Gaussian error at depth. This is detailed in Sect. 3.
- 30 - The time window for the 3D-VAR bias correction was reduced from 3 to 1 month to
31 obtain a correction that is more in line with the current physics, which is made possible by
32 the good spatial and temporal distribution of the Argo network from 2006.
- 33 - In the previous system PSY4V2, the SSH increment was the sum of barotropic and
34 baroclinic (dynamic) height increments. Dynamic height increment was calculated from



1 the temperature and salinity increments, while the barotropic increment was an output of
2 the analysis. In the system PSY4V3, we directly use the total SSH increment given by the
3 analysis to take into account, among other things, the wind effect like the hydraulic
4 control near the straits (Song, 2006; Menemenlis et al., 2007).

5 - The uncertainties in the MDT estimate and the sparsity of the observation networks (both
6 altimetry and in situ profiles) on the 7-day assimilation window do not allow to accurately
7 estimate the observed global mean sea level. Moreover, the mean sea level time evolution
8 is the result of an imposed trend for mass inputs (2.2 mm yr^{-1} , see Sect. 2.1) together with
9 a diagnostic steric effect re-computed from model T and S. Therefore, the global mean
10 increment of the total sea surface height is set to zero and the mean sea level is not
11 controlled by data assimilation.

12 - The error covariance matrices needed for data assimilation are defined using anomalies of
13 the different variables coming from a simulation in which only a 3D-VAR large scale bias
14 correction of T, S has been performed (instead of using a free run as was done in the
15 previous system PSY4V2). Moreover, these anomalies are spatially filtered in order to
16 retain only the effective model resolution and in order to avoid injecting noise in the
17 increments. This is detailed in Sect. 3.

18 **2.3 Additional Quality Controls on in situ observations**

19 To minimize the risk of erroneous observations being assimilated in the model, the system
20 PSY4V3 carries out two successive Quality Controls (QC1 and QC2) on the assimilated T
21 and S vertical profiles. These are done in addition to the quality control procedures performed
22 by the data producers.

23 **2.3.1 Quality Control QC1**

24 The first quality control QC1 has been already described in Lellouche et al. (2013) and can be
25 summarized as follows. An observation is considered suspicious if the two following
26 conditions are both satisfied:

$$27 \quad \begin{cases} |innovation| > threshold \\ |observation - climatology| > 0.5 * |innovation| \end{cases} \quad (1)$$

28

29 where the spatially and seasonally varying *threshold* value comes from statistics (mean,
30 standard deviation) computed with the very large number of temperature and salinity



1 innovations collected in the Mercator GLORYS2V1 (GLobal Ocean ReanalYsis and
 2 Simulation – stream 2 – version 1) reanalysis (1993-2009). This first QC allows the detection
 3 of spikes and large biases.

4 **2.3.2 Quality Control QC2**

5 The second quality control QC2 is based on dynamic height innovation (vertical integration
 6 from the surface to the bottom) statistics and allows detecting small biases which are present
 7 on the whole water column, and thus can induce large errors. It basically says that the thermal
 8 or haline component of dynamic height innovation ($hdyn(innov_T)$ or $hdyn(innov_S)$) cannot
 9 exceed some threshold in height ($threshold_T$ for thermal component or $threshold_S$ for haline
 10 component). It can be summarized as follows. A vertical profile is rejected if the following
 11 condition is satisfied:

$$12 \quad \left\{ \begin{array}{l} \text{For temperature : } \frac{|C * hdyn(innov_T)|}{\sum dz_T} > threshold_T \\ \text{For salinity : } \frac{|C * hdyn(innov_S)|}{\sum dz_S} > threshold_S \end{array} \right. \quad (2)$$

$$13 \quad \text{where } \left\{ \begin{array}{l} C = 200 / \sum dz \quad \text{if } 0 < \sum dz \leq 200 \\ C = 500 / \sum dz \quad \text{if } 200 < \sum dz \leq 500 \\ C = \sum dz \quad \text{if } \sum dz > 500 \end{array} \right. \quad (3)$$

14 and dz_T is the model layer thickness corresponding to the temperature observation (same for
 15 dz_S and salinity). These last conditions (Eq. (3)) prevent the threshold from being reached too
 16 quickly in shallow areas.

17 The average and standard deviation of the thermal or haline components of dynamical height
 18 innovation have been calculated from a global simulation at $1/4^\circ$, which is a twin simulation
 19 of the PSY4V3 one. Note that the simulation at $1/4^\circ$ also assimilates the CORA 4.1 CMEMS
 20 in situ database. The temperature and salinity threshold 2D fields used by QC2 are then
 21 computed as the average plus six times the standard deviation of the dynamical height
 22 innovations (Fig. 2). With these temperature and salinity thresholds, the system will reject
 23 more easily biased salinity profiles in the tropics and biased temperature profiles in strong
 24 currents.
 25

26 It should also be noted that the QC2 quality control rejects the entire vertical profile while the
 27 QC1 quality control only rejects aberrant temperature and/or salinity values at some given
 28 depths on the vertical profile.
 29



1 Figure 3a shows an example of a “wrong” temperature profile detected by the QC2 (and not
2 by the QC1) at the end of July 2008. In this case, $threshold_T$ is equal to 0.3 m (Fig. 3b). The
3 first condition of Eq. (2) is satisfied and the profile is rejected. When this profile is
4 assimilated (simulation without QC2), abnormal temperature RMS innovation values appear
5 at the temporal position (July 2008) of this profile in the Azores region (Fig. 3c). Using QC2
6 quality control allows solving the problem for this particular profile but also for some others
7 profiles (see Fig. 3c).

8 Statistics of the QC1 and QC2 quality controls are summarized in Fig. 4, where the
9 percentage of suspicious temperature and salinity profiles is given as a function of the year
10 over the 2007-2016 period. This percentage is relatively stable for both temperature and
11 salinity profiles, with little year-to-year variability, except for the years 2012 and 2013 where
12 more suspicious temperature and salinity profiles than usual were detected. Nevertheless, this
13 percentage remains relatively low (less than 0.35 % for temperature and 3.5 % for salinity),
14 knowing that the number of temperature profiles available each year ranges between 1.1
15 million and 1.7 million and the number of salinity profiles between 150,000 and 600,000.

16

17 **3 Impact of major updates**

18 Most of the deficiencies in the systems can be related to these main recurring problems:
19 initialization, atmospheric forcing biases, abyssal circulation and efficiency of the
20 assimilation schemes. The first three problems are related to uncertainties in poorly observed
21 areas or parameters (i.e. deep ocean, ice thickness) and to intrinsic errors of the atmospheric
22 forcing. The last problem is related to linearity and stationarity hypotheses in the assimilation
23 schemes. In this section, we detail the solutions adopted for the system PSY4V3, reducing
24 uncertainties in the thermohaline component and allowing flow dependence in our
25 assimilation scheme.

26 **3.1 Initialization of oceanic simulation**

27 One way to initialize physical ocean model simulations is by using climatological values of
28 temperature and salinity from databases and assuming the velocity field is zero at the start.
29 The model physics then spins up a velocity field in balance with the density field. Another
30 common way to initialize a model is with fields from a previous run of that model, or with the
31 results from another model.



1 Given that data assimilation of the current observation network rapidly (in about 3 months)
2 adjusts the model state in the first 1000 m, the first solution has been chosen to avoid potential
3 drifts occurring after some years of simulation. Compared with the previous system PSY4V2
4 starting in October 2012 from the WOA09 3D climatology (see Fig. 1), the PSY4V3 system
5 starts in October 2006 using improved initial climatological conditions. For that, we chose to
6 use ENACT-ENSEMBLES EN4 1° global product (Good et al., 2013) which consists in
7 monthly objective analyses. The great interest of these monthly fields is that a 3D observation
8 weight (between 0 and 1) describes the influence of the observations for each field. This
9 information helps to retain only the observed points and not the perpetual climatology. This
10 allows the computation of validated trends for each month and of climatology for a particular
11 date. For that, a pointwise linear regression and in particular the Kendall's robust line-fit
12 method (Hoaglin et al., 1983) is used, allowing us to obtain an initial condition called "robust
13 EN4" for any time based only on real observations.

14 Two free simulations (without any data assimilation) have been performed with the system
15 PSY4V3, using either WOA09 or robust EN4 as initial condition in October 2006. Figure 5
16 shows the box-averaged innovations of temperature and salinity as a function of time and
17 depth over the October 2006 - December 2007 period. The top left panel reveals that, using
18 WOA09 as initial condition, a fresh bias appears in the first 100 meters of the innovation,
19 particularly more pronounced at the surface. It is not anymore the case when using robust
20 EN4 to initialize the model (top right panel). For temperature, the bottom left panel exhibits
21 cold biases above 100 m and below 300 m that are considerably reduced by using robust EN4
22 as initial condition (bottom right panel). The warm bias between 200 m and 300 m is slightly
23 reinforced but it concerns only the top 300 m and this will be corrected by the assimilation of
24 Argo profiles. Deeper biases are reduced with this new initialization.

25 **3.2 Correction of precipitations**

26 Many studies (e.g. Janowiak et al., 1998; Janowiak et al., 2010; Kidd et al., 2013) have
27 compared reanalysis and atmospheric model precipitation fields with observation-based
28 datasets, and have shown that atmospheric model products always bring significant and
29 systematic errors, and are not able to close the global average freshwater budget. For instance,
30 Janowiak et al. (2010) found that the IFS operational model and ERA-Interim reanalysis (Dee
31 et al., 2011) from ECMWF perform well for temporal variability with respect to observational
32 datasets, but they globally overestimate the daily precipitations. Although progresses have



1 been made in the ECMWF forecast model, substantial errors still occur in the tropics (Kidd et
2 al., 2013). The correction of atmospheric forcing within ocean applications has already been
3 successfully explored by adjusting atmospheric fluxes via observational datasets in global
4 applications (Large and Yeager, 2009; Brodeau et al., 2010). Other studies only focused on
5 precipitation correction (Troccoli and Kallberg, 2004; Storto et al., 2012).

6 The proposed method in this paper consists of correcting the daily precipitation fluxes by
7 means of a monthly climatological coefficient, inferred from the comparison between the
8 Remote Sensing Systems (RSS) Passive Microwave Water Cycle (PMWC) product (Hilburn,
9 2009) and the IFS ECMWF precipitations. We use remote PMWC product because of its
10 relative high $1/4^\circ$ resolution able to represent more accurately narrow permanent features such
11 as the Intertropical Convergence Zone. The use of spatially varying monthly climatological
12 coefficient is justified by the fact that the inter-annual variability is well captured by the
13 ECMWF forecast model and allows us to apply the correction outside the special sensor
14 microwave/imager era. This latter assertion is a limitation of the method as it assumes the
15 operational ECMWF forecast model has a constant bias. In order to avoid discontinuities
16 when either PMWC or ECMWF products exhibit zero precipitation, e.g. in arid areas, we do
17 not apply any correction in monthly mean values less than 1 mm of rainfalls fluxes. Also, in
18 order to keep the more accurate small-scale signal from the high resolution forcing, the
19 correction is only applied to large-scale component obtained by a low-pass Shapiro filter.
20 Hilburn et al. (2014) provided accuracy of RSS over ocean rain retrievals validated against
21 well established long-term in situ datasets such as observations from Pacific Marine
22 Environment Laboratory rain gauges on moored buoys in the tropics. They found that on
23 monthly averages, the standard deviation between satellite and buoy is 15.5 %. The
24 differences are greatest in the Indian Ocean and Western Pacific. We then arbitrarily capped
25 the correction beyond 20 % in order to take into account these satellite-based retrievals errors.
26 Lastly, we did not apply the correction poleward 65° N and 60° S because of lack and
27 important biases of satellite-based precipitations estimate (Lagerloef et al., 2010) at high
28 latitudes.

29 Figure 6 represents the difference between the IFS precipitations coming from ECMWF and
30 the PMWC product using satellite data, before and after large scale correction. Original IFS
31 forcings exhibit a systematic over-estimation of precipitation within the inter-tropical
32 convergence zones (up to 3 mm day^{-1}) and under-estimation at mid- and high-latitudes (up to
33 -4 mm day^{-1}). After correction, the mean bias compared with PMWC is reduced from 0.47 to
34 0.19 mm day^{-1} .



1 To validate this correction, two global ocean hindcast simulations of several years, using only
2 the 3D-VAR large-scale biases correction in temperature and salinity, have been performed,
3 one with IFS correction and the other without. Figure 7 represents the mean surface salinity
4 innovation (difference between the assimilated observation and the model) on the year 2011.
5 These maps demonstrate that the IFS correction is beneficial in many areas, reducing the
6 magnitude of the near-surface salinity fresh mean bias in the Tropics down to 0.5 psu.

7 **3.3 Assimilation of climatological temperature and salinity climatology in the** 8 **deep ocean**

9 Due to unresolved processes (internal waves, spurious mixing in overflow regions, tidal
10 mixing) and inaccurate atmospheric forcing (bulk formulas), the model may drift at depth.
11 Unfortunately, there are very few temperature and salinity profiles below 2000 m to constrain
12 the model drift. Hence, the climatology is currently the only source of information at depth to
13 prevent the model from drifting. Virtual vertical profiles of temperature and salinity below
14 2000 m are built from the monthly WOA13v2 climatology. These virtual observations are
15 geographically positioned on the model horizontal grid with a coarse resolution ($1^\circ \times 1^\circ$) and
16 on the model vertical levels from 2200 m to the bottom.

17 As in Greiner et al. (2006), we define empirically the standard deviations (departures from the
18 climatology) σ_T for temperature and σ_S for salinity, as a simple linear vertical profile:

$$19 \quad \begin{cases} \sigma_T = \text{MAX} \left(\left(\frac{0.6-z/10^4}{3} \right); 0.05 \right) \\ \sigma_S = \sigma_T / 8 \end{cases} \quad (4)$$

20 where z is the depth (in meters).

21 We define then σ_{TS} the density departure from the climatology:

$$22 \quad \sigma_{TS} = \alpha \sigma_T + \beta \sigma_S \quad (5)$$

23 where α represents the thermal expansion coefficient and β the saline contraction coefficient.
24 Following Jackett and McDougall (1995), these coefficients are assumed to depend only on
25 latitude and depth of the ocean as illustrated by Fig. 8.

26 If we note d_{TS} the density innovation, d the temperature or the salinity innovation and σ the
27 temperature or the salinity departure from the climatology, the value of the climatological
28 error e is prescribed as:



$$\begin{cases}
 \text{If } |d_{TS}| \leq 2\sigma_{TS} \text{ then } e = \infty \text{ (observation rejected)} \\
 \text{If } |d_{TS}| > 2\sigma_{TS} \text{ then } \begin{cases}
 \text{if } 2\sigma < |d| < 3\sigma \text{ then } e = \text{MIN}\left(\frac{2\sigma}{3}\left(\frac{|d|}{|d|-2\sigma}\right); 20\sigma\right) \\
 \text{if } |d| \geq 3\sigma \text{ then } e = 2\sigma \\
 \text{if } |d| \leq 2\sigma \text{ then } e = 20\sigma
 \end{cases}
 \end{cases} \quad (6)$$

2
 3 A non-Gaussian error is used to impose a weak constraint on the model at depth (Fig. 9). That
 4 way, we correct the model drift without constraining a slow moderate variability or trend.
 5 Basically, the hypothesis is that small to medium departures from the climatology (2σ or less)
 6 has an even probability. For instance, a $0.2\text{ }^\circ\text{C}$ model warming at 2000 m due to a positive
 7 North Atlantic Oscillation pattern must not be corrected as zero. Indeed, a $0.2\text{ }^\circ\text{C}$ cooling is as
 8 likely as the warming, since the climatology is the time average of those anomalies. So, only
 9 large departures from climatology (3σ or more) should be corrected. It corresponds to highly
 10 unlikely events that are typical of model drifts. An interesting point is that model drift is often
 11 corrected locally, downstream the outflow, before it spreads out (see Fig. 10). Ideally, it gives
 12 a little regional correction instead of a large basin scale bias.

13 To validate this kind of assimilation, two global ocean simulations of several years, using
 14 only the 3D-VAR large-scale biases correction in temperature and salinity, have been
 15 performed. Due to the high computational cost of the system PSY4V3, the assimilation of
 16 WOA13v2 below 2000 m has been tested with a global intermediate-resolution system at $\frac{1}{4}^\circ$,
 17 which is, in all other aspects, very close to the high resolution system PSY4V3. All in situ
 18 observations have been used as well.

19 In practice, the assimilation of WOA13v2 climatological profiles below 2000 m in the system
 20 concerns mostly some regions where the steep bathymetry might be an issue for the model
 21 (Kerguelen Plateau, Zapiola Ridge, and Atlantic ridge). Figure 10 shows mean temperature
 22 (left) and salinity (right) innovations (WOA13v2 climatological profiles minus model) in
 23 2013 at 2865 m. The assimilation of these climatological profiles occurs more or less at the
 24 same locations over the time period 2007-2016. Since the conditions of the system of
 25 equations (6) relate to the density innovation, we have a perfect symmetry of the temperature
 26 and salinity data which are assimilated. This has the effect of not disturbing the density
 27 gradients too much.

28 If we focus on latitudes between 30° S and 60° S , Fig. 11 represents temperature (top panels)
 29 and salinity (low panels) annual anomalies over depth (500 - 5000 m) and time (2007-2014).
 30 The simulation on the left does not assimilate climatological vertical profiles while the



1 simulation on the right assimilates some. These maps demonstrate that the assimilation of
2 WOA13v2 below 2000 m is beneficial, reducing drifts below 2000 m. In the Antarctic
3 Circumpolar Current (ACC), the assimilation of these profiles makes it possible to maintain,
4 for instance, the Antarctic Bottom Water (see Gasparin et al., 2018 - Submitted in Journal of
5 Marine Systems). This also impacts the vertical repartition of the steric height, without
6 degrading the quality of the results comparing with profiles from the Argo network.

7 **3.4 Construction of the forecast error covariance**

8 The seasonally varying forecast error covariance is based on the statistics of a collection of
9 3D ocean state anomalies. This approach is based on the concept of statistical ensembles in
10 which an ensemble of anomalies is representative of the error covariance. In this way,
11 truncation no longer occurs and all that is needed is to generate the appropriate number of
12 anomalies. The way in which these anomalies are computed from a long numerical
13 experiment is described in Lellouche et al. (2013). In the previous system PSY4V2, a free
14 simulation was used to calculate the anomalies. For the system PSY4V3, the anomalies are
15 computed from a simulation in which only a 3D-VAR large scale bias correction of T/S has
16 been performed. In the following section, we evaluate the potential added value of this choice
17 on the quality of the analysis increments.

18 **3.4.1 Choice of the simulation from which to calculate the anomalies**

19 The system PSY4V3 was run over the October 2006 – October 2016 period to catch-up the
20 real-time (“OPER” simulation), starting from 3D temperature and salinity initial conditions
21 based on the EN4 climatology. This simulation benefited from the full data assimilation
22 system, including the 3D-VAR biases correction and the SAM filter. Two other simulations
23 over the same period have been performed. The first one is a “FREE” simulation (without any
24 data assimilation) and the second one has exactly the same model tunings but only benefits
25 from the temperature and salinity 3D-VAR large-scale biases correction (“BIAS” simulation).

26 Figure 12 and Figure 13 show comparisons between this triplet of PSY4 simulations and two
27 observational products. The first product is the CMEMS/DUACS (Data Unification and
28 Altimeter Combination System) Merged-Gridded Sea Level Anomalies heights in delayed
29 time on a $\frac{1}{4}^\circ$ regular horizontal grid with a 1-day temporal resolution (Pujol et al., 2016). The
30 second one is the Roemmich-Gilson Argo monthly climatology on a 1° regular horizontal grid
31 (Roemmich and Gilson, 2009) which is commonly used in the oceanographic community.



1 Figure 12a,b,c shows the 2007-2015 SSH variability for the three simulations. SSH variability
2 difference is defined as the difference of SSH standard deviations from PSY4 simulations and
3 the DUACS product (Fig. 12d,e,f). Comparing to the variability of the DUACS product, the
4 fronts in high mesoscale variability regions such as the Gulf Stream, the Kuroshio, the
5 Agulhas current or the Zapiola eddy are misplaced in the FREE simulation. In the BIAS
6 simulation, these fronts are better positioned due to the large-scale correction of temperature
7 and salinity. However, this simulation presents more energy compared to DUACS, apart of
8 the main fronts. This corresponds to a leakage of vorticity from the fronts due to the mean
9 advection. Note that the gridded DUACS product also underestimates the variability as
10 wavelengths smaller than 200 km are barely resolved in the gridded fields. The mesoscale
11 features are well constrained in the OPER simulation with the information coming from
12 satellite data.

13 Time-averaged density differences along the equatorial Pacific between two ENSO events
14 (“Oct-Dec 2008 minus Oct-Dec 2009”), computed from the PSY4 simulations and from the
15 Roemmich-Gilson Argo monthly Climatology, are shown in Fig. 13. The SCRIPPS Argo
16 product presents a higher density difference in the eastern part of the equatorial Pacific. It
17 corresponds to the change from moderate La Niña conditions early 2008 to moderate El Niño
18 conditions in 2009. The FREE simulation is not dense enough in the east compared to
19 observations particularly at the pycnocline depth (1025 kg/m^3 isopycn). The BIAS simulation
20 intensifies the density difference. The OPER simulation gets even closer to the SCRIPPS
21 Argo product. There is also an upward tilt of the density difference maximum in agreement
22 with the observations.

23 In summary, the BIAS simulation better represents the density fronts on the horizontal (Gulf
24 Stream) and on the vertical (Pacific pycnocline). The covariance matrix deduced from this
25 simulation has information on the density gradients that is well placed. This is valuable off the
26 equator though geostrophy, and at the equator to control the zonal pressure gradient. The
27 variance in sea level is stronger than the DUACS one (see Fig. 12e) but the most important
28 point for the construction of the anomalies is to have well-placed density gradients. In the
29 OPER simulation and as mentioned in Lellouche et al. (2013) in the description of the data
30 assimilation system SAM, an adaptive scheme will correct the variance and will give an
31 optimal model error variance based on a statistical test formulated by Talagrand (1998).



1 **3.4.2 Anomaly filtering**

2 The signal at a few horizontal grid “ Δx ” intervals in the model outputs on the native full grid
3 is not physical but only numerical (Grasso, 2000) and should not be taken into account when
4 updating an analysis. This is why several passes of a Shapiro filter have to be applied at the
5 anomalies computation stage in order to remove the very short scales that in practice
6 correspond to numerical noise. This can also help to filter out the noise from the covariance
7 matrix due to the sampling error (Raynaud et al., 2009).

8 To illustrate the impact of the anomaly filtering, we set up some experiments consisting in the
9 assimilation of a single altimeter track with different levels of filtering. These experiments
10 have been performed with a Mercator Ocean regional system at $1/12^\circ$ using the SAM data
11 assimilation scheme, in order to reduce the high computing cost of the system PSY4V3 as
12 well as the time consuming to build different sets of anomalies at the global scale. Figure 14
13 shows SLA increments obtained with these different levels of anomaly filtering. It should be
14 noted that the anomaly filtering has a direct effect on the analysis increment, since the latter is
15 a linear combination of the anomalies.

16 Figure 14a represents SLA innovation along the single assimilated track. Figure 14b,c,d
17 represents the SLA increments obtained respectively with 10, 100 and 300 Shapiro passes as
18 the anomaly filtering mentioned above (corresponding approximately to a 3, 10 and 15
19 horizontal grid “ Δx ” intervals filter). We can see that the correction on the track remains more
20 or less the same. The strongest differences occur outside the track where the innovation
21 information is extrapolated.

22 Other experiments, closer to real time integration set up have been performed, assimilating all
23 the altimeter tracks available on a 7-day assimilation window, instead of one single track.
24 Figure 15 shows the SLA increments difference using 10 and 300 Shapiro passes as anomaly
25 filtering. The conclusions are the same as those concerning the experiments with a single
26 assimilated track. The correction on the tracks remains almost the same for the two levels of
27 filtering as small differences appear along the tracks. The strongest differences occur outside
28 the tracks where the innovation information is extrapolated to fill the gaps. Unfiltered
29 increments have small-scale structures that are statistical artifacts. Small structures can
30 cascade in the model, and stay trapped between the repetitive tracks, without correction by the
31 assimilation. This happens less when the filtering is performed on the anomalies beyond the
32 effective resolution of the model.



1 **3.5 Adaptive tuning of observation errors**

2 In order to refine the prescription of observation errors (instrumental and representativity
3 errors), adaptive tuning of observation errors for the SLA and SST has been implemented in
4 PSY4V3. The method has not been used for temperature and salinity vertical profiles because
5 of the reduced number of in situ data compared with satellite data. Then, 3D fixed observation
6 errors are used for the assimilation of in situ temperature and salinity vertical profiles. The
7 method consists in the computation of a ratio, which is a function of observation errors,
8 innovations and residuals (Desroziers et al., 2005). It helps correcting inconsistencies on the
9 specified observation errors. This ratio can be expressed as:

$$10 \quad \mathbf{ratio} = \frac{\mathbf{residual}(\mathbf{innovation})^T}{\mathbf{observation\ error}} \quad (7)$$

11

12 Ideally, *ratio* is equal to 1. When the ratio is less (respectively larger) than 1, it means that
13 the observation error is overestimated (respectively underestimated). The objective of this
14 diagnostic is to improve the error specification by tuning an adaptive weight coefficient acting
15 on the error of each assimilated observation. As a first guess of the method, the initial
16 prescribed observation error matches the one used in the previous system (Lellouche et al.,
17 2013) where the observation error variance was increased near the coast and on the shelves
18 for the assimilation of SLA, and increased only near the coast (within 50 km of the coast) for
19 the assimilation of SST.

20 Figure 16 represents the temporal evolution of the ratio defined in Eq. (7) for Envisat satellite.
21 At the beginning of the simulation, the observation error is overestimated (ratio less than 1).
22 The ratio tends to 1 after only a few weeks of simulation.

23 For SLA (Fig. 17), the a priori prescribed observation error is globally significantly reduced.
24 The median value of the error changed from 5 cm to 2.5 cm in a few assimilation cycles and
25 allows for better results. This method allows us to have more realistic and evolutive
26 observation error maps which can provide valuable information for the space agencies.

27 The realism of tropical oceans is crucial for seasonal forecasting applications. Tropical
28 Instability Waves (TIWs) can be diagnosed from SST (Chelton et al., 2000). These Kelvin
29 Helmholtz waves initiate at the interface between areas of warm and cold sea surface



1 temperatures near the Equator and form a regular pattern of westward-propagating waves.
2 Figure 18 gives an example of adjustment of the observation error to the model physics and
3 atmospheric variability. The SST anomalies in the equatorial Pacific clearly show the
4 propagation westwards of TIWs in the second half of the year. This is more pronounced
5 during episodes of La Niña (mid-2007 and mid-2010). The observation error anomalies
6 estimated by “Desroziers method” show that the error increases when these TIWs are more
7 marked. This can be explained by uncertainties in SST observations (clouds) and model shift
8 of the TIWs structures. The error decreases in the reverse case.

9 We have also performed an Empirical Orthogonal Function (EOF) analysis to assess the
10 variability of the SST observation error (Fig. 19). Mode 1 is associated to the seasonal cycle
11 and mode 2 (not shown) corresponds to the migration of the seasonal signal. Mode 3 is
12 associated to the inter-annual signal with for instance the transition La Niña / El Niño,
13 showing that the SST error is able to adapt both to the seasonal and inter-annual fluctuations.

14

15 **4 Scientific assessment**

16 This section describes the PSY4V3 system’s quality assessment with diagnostics over
17 particular years, together with time series over multiyear periods. To evaluate the quality of
18 the system, the departure from the assimilated observations (SST, SLA, T/S vertical profiles
19 and sea ice concentration) is measured. Moreover, the analyses are also compared with
20 observations that have not been assimilated by the system such as tide gauges, velocity
21 measurements from drifting buoys, NOAA SST and AMSR sea ice concentration. NOAA
22 SST and AMSR sea ice analyses are not fully independent, since the upstream observations
23 are the same than for assimilated CMEMS OSTIA SST and OSI Sea Ice concentrations, but
24 comparisons to a variety of estimates using different algorithms and protocols provides a
25 useful consistency analysis.

26 **4.1 SST**

27 **4.1.1 Assimilated SST**

28 OSTIA product is assimilated in the system PSY4V3. Compared to the previous system
29 PSY4V2, some large scale cold biases with respect to OSTIA are reduced in the Indian,
30 Eastern South Pacific, and western North Pacific (not shown). On the other hand, warm biases
31 are not reduced, especially in regions of strong inter-annual warm events such as the Eastern



1 Tropical Pacific where strong El Niño took place in 2015/2016, but also in the ACC, the Gulf
2 Stream and the Greenland Current (Fig. 20a). Some inconsistencies can be found between
3 OSTIA SST and in situ near surface temperature, particularly in the North Pacific where the
4 system PSY4V3 presents a cold bias compared to in situ near surface temperature but a warm
5 bias compared to OSTIA SST (Fig. 20b). Figure 20c shows the difference between drifting
6 buoys SST and the system PSY4V3 over the year 2015. The drifting buoys SST data are
7 present in the CMEMS in situ database used by Mercator but they have not been assimilated
8 in the system because the depth of these data is a nominal value and we chose to assimilate
9 only data with a measured depth value. Although we plan to assimilate these data in the future
10 system, we use currently this data as independent information. This allows us to see that SST
11 from in situ vertical profiles and SST from drifting buoys are coherent with each other. We
12 thus find again the cold bias highlighted by the comparison with SST from in situ vertical
13 profiles in the North Pacific.

14 We checked also the time series of the mean and the RMS of the misfit (innovation) between
15 the observed SSTs and the model. For OSTIA SST, we obtain a mean warm bias of -0.1 °C
16 and a RMS error of 0.45 °C (Fig. 21). Seasonal fluctuations of the SST biases on global
17 average can be seen as a lack of stratification in the model, which causes stronger mid-latitude
18 warm biases during (boreal) summer (and a warm bias between 50 m and 100 m). For in situ
19 SST, the bias is smaller, suggesting that OSTIA might be colder than in situ near surface
20 observations on global average. We can notice a drop in the RMS of in situ surface data in
21 January 2014, which is due to the use of near real time observations, where most of the
22 surface observations do not have sufficient quality flag.

23 **4.1.2 Comparison with an independent SST product**

24 CLS (Collecte Localisation satellites) operates since 2002 a near real time oceanography data
25 service named CATSAT, for scientific, institutional or private users (support to fishery
26 management or to the offshore oil and gas industry). These data include satellite observations
27 as chlorophyll-a, SST and altimetry. Maps of SST are computed from Aqua/MODIS, S-
28 NPP/VIIRS and Metop/AVHRR infra-red sensors at 2 km resolution, using nighttime data
29 only to avoid diurnal warming effects. We can then evaluate the system ability to produce the
30 mesoscale by comparing with the CATSAT daily SST product. On Fig. 22, the CATSAT
31 daily snapshot can be considered as an independent dataset since the OSTIA SST assimilated
32 in the system has mostly seen microwave measurements during two weeks, as it was very



1 cloudy in the Gulf of Mexico. 31st of March 2016 is the first clear day showing well, from
2 infrared measurements, the Loop Current and other structures in the western part of the Gulf
3 of Mexico. The Loop Current is almost forming a closed meander. This is reproduced by the
4 system PSY4V3, as well as secondary structures like the filament in the North (Fig. 22).
5 Visible limitations of this 1/12° system concern the fine sub-mesoscale that can not be
6 resolved, and the lack of tidal mixing along Yucatan coasts (Kjerfve, 1981).

7 **4.2 Temperature and salinity vertical profiles**

8 For the T/S vertical profiles, we checked time series of the RMS of the difference between the
9 model analysis and the observations, for temperature on the left and for salinity on the right
10 (Fig. 23) in the whole water column. We compare observation and – climatology (red line),
11 previous system PSY4V2 (blue line), new system PSY4V3 (black line).

12 On global average, and compared to the previous system PSY4V2, the system PSY4V3
13 slightly degrades the temperature statistics (-0.03 °C) but it significantly improves the salinity
14 statistics by decreasing the 0-5000 m RMS salinity by 0.1 psu. This allows a more accurate
15 description of the water masses. This better balance arises from the new in situ errors that give
16 more weight to the salinity data (not shown). We can also notice that the systems are always
17 better than the climatology. The comparison to climatology is a minimum performance
18 indicator that the system must achieve. The differences with the climatology are worst from
19 the beginning of the year 2013. It can be explained by the fact that six different decades of
20 WOA13v2 monthly climatology can be found on the NODC website. We chose the available
21 2005-2012 decade (near of our time period simulation). So, in situ temperature and salinity
22 vertical profiles we assimilated in the system are coherent with this WOA13v2 product until
23 the end of year 2012 and this is no longer the case after.

24 Moreover, the system PSY4V3 experiences a slight warm bias (negative observation minus
25 forecast difference) in subsurface (25 - 500 m) on global average (not shown). For the year
26 2015, part of this signal comes from the strong inter-annual ENSO signals in the Tropical
27 Pacific where the near surface bias is also warm, as well as in the ACC and the Gulfstream.
28 Seasonal cold surface biases appear in the mid latitudes, linked with a lack of stratification
29 during summer. Summer warming is injected too deep and results in subsurface spurious
30 warming and too shallow mixed layer. However, these biases remain small on global average.



1 **4.3 Sea Level**

2 **4.3.1 Assimilated SLA**

3 The system PSY4V3 is closer to altimetric observations than the previous one with a global
4 forecast RMS difference of around 6 cm instead of 7 cm for the system PSY4V2 (not shown).
5 This RMS difference is consistent with the observations errors (about 2 cm for altimeters and
6 4 cm for MDT). The statistics come from the data assimilation innovations computed from the
7 forecast used as the background model trajectory, and give an estimate of the skill of the
8 optimal model forecast. These scores are averaged over all seven days of the data assimilation
9 window, which means the results are indicative of the average performance over the seven
10 days, with a lead time equal to 3.5 days.

11 More precisely, on the year 2015, the SLA mean and RMS errors are considerably reduced in
12 the new system PSY4V3 compared to the previous one (Fig. 24). The mean bias is reduced by
13 0.3 cm (from -0.8 cm to 0.5 cm) and the RMS is reduced by 2.4 cm (from 7.9 cm to 5.5 cm).
14 This is mainly due to the use of the “Desroziers” method to adapt the observations errors
15 online, which yields to more information from the observations being used (see Sect. 3.5).
16 These improvements occur in nearly all regions of the ocean but are more pronounced in
17 some regions (e.g. North Atlantic, Hudson Bay, Labrador Sea). In some others regions (e.g.
18 Indonesian or west tropical Pacific), it remains some errors in sea level linked to the
19 uncertainty in the MDT or missing parametrisations in the model (interaction wave-current,
20 tides).

21 **4.3.2 Comparison to tide gauge data**

22 The system PSY4V3 produces hourly outputs at the surface that can be compared with tide
23 gauge measurements. For that, we used the BADOMAR product which is a specific processed
24 tide gauges database developed and maintained at CLS and consists of filtered tide gauge data
25 from the GLOSS/CLIVAR “fast” sea level data tide gauge network. These tide gauge data are
26 corrected from inverse barometer effect and tides. High frequency model SSH compares well
27 with tide gauges in many places, with a slight improvement in PSY4V3 with respect to
28 PSY4V2 (not shown). The best agreement between the system PSY4V3 and tide gauges is
29 found in the tropical band, as can be seen in Fig. 25, while shelf regions and closed seas are
30 less accurate. This confirms the latitude dependence of the correlation between tide gauges
31 and satellite altimetry or modelled SSH discussed in Vinogradov and Ponte (2011) or
32 Williams and Hugues (2013).



1 The improvements related to water masses and SLA lead to a correct Global Mean Sea Level
2 (GMSL) trend. We checked the system GMSL by comparing the results with recent estimated
3 trend from the paper of Chambers et al. (2017). We found for the model a trend of 3.2 mm yr⁻¹
4 over the PSY4V3 simulation time period which is coherent with DUACS value (3.17 ± 0.67
5 mm yr⁻¹). Moreover, the temporal evolution of the global mean model SSH is coherent and
6 phased with the observations.

7 **4.4 Sea ice concentration**

8 **4.4.1 Assimilated sea ice concentration**

9 The system PSY4V3 assimilates OSI SAF sea ice concentration in both hemispheres with a
10 monovariate/monodata scheme. As expected, PSY4V3 is closer to the observations than the
11 previous system PSY4V2 (not shown), in which no sea ice observations had been assimilated.
12 As illustrated by Fig. 26, the system PSY4V3 has a slight overestimation of ice during the
13 melting season in summer (up to 3 % on average in both hemispheres). Conversely, the mean
14 error is stronger on average during winter (10 to 20 % underestimation, depending on the
15 year). RMS errors are also larger during summer (up to 20 % in the Arctic and 30 % in the
16 Antarctic with respect to OSI SAF observations), and drop to less than 10 % in winter. These
17 RMS errors quantify the capacity of the system to capture weekly time changes in the ice
18 cover.

19 We have also checked the evolution of the sea ice volume diagnosed by the system PSY4V3
20 which assimilates observations of sea ice concentration with a monovariate/monodata scheme.
21 The data assimilation scheme SAM produces increment of sea ice concentration which is the
22 unique sea ice correction applied in the model using the Incremental Analysis Update (IAU)
23 method described in Lellouche et al. (2013). The sea ice volume then adjusts to this correction
24 considering a constant sea ice thickness. No sea ice thickness observations are assimilated in
25 the system. The risk is therefore to obtain unrealistic drifts or trends of the unconstrained sea
26 ice volume. Presently, sea ice volume retrievals from satellites are associated with large
27 uncertainties (Zygmuntowska et al., 2014). Consequently, modelled sea ice volume is difficult
28 to validate and one of the solution is to compare modelled sea ice volume from several
29 systems.

30 Figure 27 shows the 2007-2016 evolution of sea ice volume for the system PSY4V3, the
31 PIOMAS modelled product (Schweiger et al., 2011) and the CMEMS GREP (Global



1 Reanalysis Ensemble Product, <http://marine.copernicus.eu/documents/QUID/CMEMS-GLO->
2 [QUID-001-026.pdf](http://marine.copernicus.eu/documents/QUID/CMEMS-GLO-QUID-001-026.pdf)) composed by four global $\frac{1}{4}^\circ$ reanalyses and the ensemble mean with the
3 associated spread from the four members. All the modelled sea ice volumes present the same
4 2007-2016 inter-annual variability. PSY4V3 and PIOMAS are included in the spread whose
5 range is reduced over time from 4,000 km³ in 2007 to 3,000 km³ from the year 2012. The
6 GLORYS2V4 reanalysis is known to have a large sea ice volume compared to other
7 reanalyses (Chevallier et al., 2017). Although we use the same method for the assimilation of
8 sea ice concentration in GLORYS2V4 and PSY4V3, the sea ice volume diagnosed by
9 PSY4V3 lies in values ranging between 13,000 and 15,800 km³, in a better accordance with
10 GREP and PIOMAS products.

11 **4.4.2 Contingency table analysis**

12 The contingency table analysis approach described in Smith et al. (2016) has been applied to
13 evaluate sea ice extent as compared to observation. Satellite ice concentration coming from
14 AMSR2 (L1B brightness with a NASA team 2 algorithm to compute sea ice concentration)
15 has been used as independent observation to provide a general assessment in the detection of
16 false alarms if ice coverage. Although this type of evaluation is usually done on forecasts, we
17 used hindcasts. For the computation of the statistics we have used a stereo-polar grid at a 20
18 km resolution. In each cell of that grid we have then computed binary values corresponding to
19 ice/open water conditions for the model and the sea ice observations by using a 40 %
20 concentration threshold. We have also restricted our study to the Proportion Correct Total
21 (PCT), following the conclusion of Smith et al. (2016), saying that it was more insightful to
22 refer to the PCT rather than others proportions. The PCT quantity is defined as $PCT = (\text{Hit ice} + \text{Hit water})/n$ (see Table 3), where n is the total number of observations with a sea ice
23 concentration greater than 15 %. A value of one corresponds to a perfect score.
24

25 Figure 28 shows times series of PCT for PSY4V2 and PSY4V3 systems. The lower PCT
26 values are due mostly to an excessive melt in spring and summer for both Arctic and
27 Antarctic. However, the assimilation of sea ice concentration improves significantly the total
28 hit rate during these periods.

29 **4.5 Currents**

30 The aim of this section is to use velocity observations which were not assimilated in the
31 system to assess the level of performance of PSY4V3 compared to the previous PSY4V2



1 system. The mean currents are checked by comparing the model to velocity observations
2 coming from Argo floats when they drift at the surface and in situ Atlantic Oceanographic and
3 Meteorological Laboratory (AOML) surface drifters. A paper by Grodsky et al. (2011)
4 revealed that an anomaly in the drogue loss detection system of the Surface Velocity Program
5 buoy had led to the presence of undetected undrogued data in the “drogued-only” dataset
6 distributed by the Surface Drifter Data Assembly Center. Rio (2012) applied a simple
7 procedure using altimeter and wind data to produce an updated dataset, including a drogue
8 presence flag as well as a wind slippage correction. We therefore used this new “drogued-
9 only” surface drifter dataset coming from CMEMS in situ TAC
10 (<http://marine.copernicus.eu/documents/QUID/CMEMS-INS-QUID-013-044.pdf>) to check
11 mean model currents.

12 Figure 29 represents zonal drift innovation for PSY4V2 and PSY4V3 systems. Although
13 some biases persist, mostly in the western tropical basins, significant improvements are
14 obtained almost everywhere with the new system PSY4V3, and more particularly in the
15 equatorial Pacific. The mean bias is reduced (from 0.1 m s^{-1} to 0.08 m s^{-1}), the South
16 Equatorial Current is slower and there is also less noise in PSY4V3. Improvements are also
17 obtained, to a lesser extent, for meridional drift (not shown). The velocities have been slightly
18 improved in terms of velocity values but also in terms of currents direction (angle between
19 observed and modelled velocities). The mean angle difference is reduced from 9.1 degrees to
20 7.2 degrees. These improvements can be attributed to the new MDT used and the more
21 adapted filtering of anomalies. However, large biases persist in the western tropical Pacific
22 (very strong in 2015 because of the strong El Niño event) with a spurious extension of the
23 northern branch of the South Equatorial Current. This is probably linked to the uncertainty
24 still present in the MDT and unresolved or missed parameterized physical processes.

25 More locally, a comparison of the 2007-2015 averaged drifts from the system PSY4V3 and
26 the observations over the Indonesian region has been performed (not shown). Currents in this
27 region are very difficult to resolve because of the many narrow straits and the strong tidal
28 mixing. The retroflexion of the westward South and North Equatorial Currents (along Papua
29 and near 12° N) into the eastward North Equatorial Counter Current (near 4° N) are well
30 reproduced structures in the Pacific. The system South Equatorial Current is a little too strong
31 at the edge of the warm pool but it is about the only weakness. The complex flow in the
32 Sulawesi Sea, the Makassar Strait and the South China Sea is well reproduced by the system.
33 The correlation is 0.70 (respectively 0.64) for the zonal (respectively meridional) velocity.



1 **5 Summary and ways for improvement of the future system**

2 The Mercator Ocean system PSY4V3, in an operational mode since October 19, 2016,
3 benefits of many important updates. PSY4V3 has a quite good statistical behaviour with an
4 accurate representation of the water masses, the surface fields and the mesoscale activity.
5 Most of the components of the system PSY4V3 have been improved compared to the
6 previous version: global mass balance, 3D water masses, sea level, sea ice and currents. Major
7 variables like sea level and surface temperature are hard to distinguish from the data.

8 In this paper, the updates showing the highest impact on the products quality have been
9 illustrated and evaluated separately. A particular focus was therefore made on the
10 initialization, the correction of precipitation, the assimilation of climatological temperature
11 and salinity in the deep ocean, the construction of the forecast error covariance and the
12 adaptive tuning of observations error.

13 Initial climatological condition has been improved in order to be more consistent with the
14 vertical profiles of temperature and salinity which has been assimilated thereafter. Rather than
15 taking directly the climatological temperature and salinity of the month corresponding to the
16 start of the simulation, we performed a pointwise linear regression, allowing to obtain an
17 initial condition at the appropriate time and based only on real observations. One-year free
18 simulations have been performed and show that biases are globally reduced.

19 Uncertainties inherent to atmospheric analyses and forecasts can induce large errors in the
20 ocean surface fluxes. For instance a slight shift in the position of a storm can induce local
21 errors in salinity, temperature and currents. In the tropical band, precipitations are
22 systematically overestimated. Moreover, large scale salinity biases can appear because the
23 global average freshwater budget is not closed. For this reason, IFS ECMWF atmospheric
24 analysed and forecasted precipitations have been corrected at large scale using satellite-based
25 PMWC product. This correction is beneficial in many areas, reducing the magnitude of the
26 near-surface salinity fresh mean bias in the Tropics down to 0.5 psu.

27 Due to unresolved process and inaccurate atmospheric forcing, the model may also drift at
28 depth. To keep some water mass properties, the DRAKKAR group used restoring of
29 temperature and salinity toward annual climatology of Gouretski and Koltermann (2004) in
30 specific areas. This choice was driven by the Antarctic Bottom Water restoring zone where
31 this climatology is recognized as the more suitable. For Mercator systems which assimilate
32 observations in a multivariate way, the problem can be more critical because of the



1 deficiencies of the background errors for extrapolated and/or poorly observed variables. To
2 overcome these deficiencies, vertical climatological T/S profiles have been assimilated below
3 2000 m using a non-Gaussian error at depth, allowing the system to capture a potential
4 climate drift in the deep ocean. In practice, the assimilation of climatological profiles below
5 2000 m in the system PSY4V3 concerns mostly some regions where the steep bathymetry
6 might be an issue for the model (Kerguelen Plateau, Zapiola Ridge, and Atlantic ridge). This
7 kind of assimilation reduces drifts below 2000 m and impacts the vertical repartition of the
8 steric height, without degrading the quality of the results comparing with the profiles from the
9 Argo network.

10 We have also proposed solutions to reduce some problems related to linearity and stationarity
11 hypotheses in the assimilation schemes. The first one concerns the construction of the forecast
12 error covariance. Rather than calculating the anomalies from a free simulation, we chose to
13 calculate them from a simulation benefiting only of the 3D-VAR large-scale biases correction
14 in temperature and salinity and representing better the density fronts on the horizontal and on
15 the vertical. Moreover, anomalies have been filtered in order to remove the scales beyond the
16 effective resolution of the model. The second one concerns the tuning of the observations
17 errors. Adaptive tuning of SLA and SST errors has been successfully implemented. It allows
18 us to have more realistic and evolutive SLA and SST error maps.

19 All these scientific and technical choices have been validated and integrated in the system
20 PSY4V3 which has been evaluated for the period 2007-2016 by means of a thorough
21 procedure involving statistics of model departures from observations. The system PSY4V3 is
22 close to SLA along track observations with a forecast (range 1 to 7 days) RMS difference
23 below 6 cm. Moreover, the correlation of the system PSY4V3 with tide gauges is significant
24 at all frequencies, however many high frequency fluctuations of the SSH might not be
25 captured by the system because tides or pressure effects are not yet included. The description
26 of the ocean water masses is very accurate on average and departures from in situ
27 observations rarely exceed 0.5 °C and 0.1 psu. In the thermocline, RMS errors reach 1 °C and
28 0.2 psu. In high variability regions like the Gulf Stream, the Agulhas Current or the Eastern
29 Tropical Pacific, RMS errors reach more than 2 °C and 0.5 psu locally. A warm bias persists
30 in subsurface, with peaks in high variability regions such as the Eastern Tropical Pacific, Gulf
31 Stream or Zapiola. Most departures from observed SST products do not exceed the intrinsic
32 error of these products (around 0.6 °C).



1 A global comparison with independent velocity measurements (surface drifters) shows that
2 the location of the main currents is very well represented, as well as their variability.
3 However, surface currents of the mid latitudes are underestimated on average. The
4 underestimation ranges from 20 % in strong currents to 60 % in weak currents. Some
5 equatorial currents are overestimated, and the western tropical Pacific still suffer from biases
6 in surface currents related to MDT biases. On the contrary the orientation of the current
7 vectors is better represented.

8 Lastly, the system reproduces the sea ice seasonal cycle in a realistic manner. However, the
9 sea ice concentrations are overestimated in the Arctic mainly during winter (due to
10 atmospheric forcing errors and too much sea ice accumulation) and in the Antarctic during
11 austral winter. They are underestimated during austral summer (too much sea ice melt and
12 errors caused by the rheology parameterization of the sea ice model). A contingency table
13 analysis approach has been also used to evaluate sea ice extent as compared to observations.
14 This approach shows clear improvements due to the assimilation of sea ice concentration in
15 the system PSY4V3.

16 Remarkable improvements have been achieved with the system PSY4V3 compared to the
17 previous version. However, some biases have been highlighted in the ocean surface features
18 as well as the 3D ocean structure at basin, sub-basin and local scales. The simulation biases
19 may be due to the initial state (especially in the deep layer where historical observation data
20 are rare), the atmospheric forcing uncertainties, the river runoff approximations, the efficiency
21 of the assimilation scheme, and the model errors induced by unresolved or parameterized
22 physical processes. Numerous projects have already been set up at Mercator Ocean to propose
23 innovative solutions. The integration of the ingredients from these projects into the future
24 CMEMS global high resolution system is planned for 2019. The improvement of numerical
25 simulations could thus be carried out, based on sensitivity tests on some model parameters
26 (e.g. coastal runoffs, atmospheric forcing, high frequency phenomena including tides, more
27 sophisticated sea ice model, interaction and retroaction between ocean currents and waves). It
28 is also planned to assimilate new types of observations in the system (drifting buoys SST,
29 higher resolution SST (L3 products), satellite sea surface salinity, velocity observations from
30 AOML surface drifters, and deep-ocean observations from Argo surface floats) to better
31 constrain the modeled variables and to overcome the deficiencies of the background errors in
32 particular for extrapolated and/or poorly observed variables. Another important issue is to use
33 a shorter assimilation time window and a 4D analysis in the assimilation scheme to better



1 correct the fast evolving processes. The next version of the global high resolution system will
2 also include seasonal errors for in situ vertical profiles already used in the CMEMS eddy-
3 resolving 1992-2016 reanalysis GLORYS at 1/12° horizontal resolution, which is based on
4 the system PSY4V3 and will appear on CMEMS catalogue in April 2018.

5

6 **References**

- 7 Amante C. and Eakins, B. W.: ETOPO1 1 Arc-minute global relief model: procedures, data
8 sources and analysis, NOAA Technical Memorandum NESDIS NGDC-24, 25 pp., 2009.
- 9 Arakawa, A. and Lamb, V. R.: A potential enstrophy and energy conserving scheme for the
10 shallow water equations, *Mon. Weather. Rev.*, 109, 18–36, 1981.
- 11 Barnier, B., Madec, G., Penduff, T., Molines, J. M., Treguier, A. M., Le Sommer, J.,
12 Beckmann, A., Biastoch, A., Böning, C., Dengg, J., Derval, C., Durand, E., Gulev, S., Remy,
13 E., Talandier, C., Theetten, S., Maltrud, M., McClean, J., and De Cuevas, B.: Impact of partial
14 steps and momentum advection schemes in a global circulation model at eddy permitting
15 resolution, *Ocean Dynam.*, 56, 543-567, 2006.
- 16 Becker, J. J., Sandwell, D. T., Smith, W. H. F., Braud, J., Binder, B., Depner, J., Fabre, D.,
17 Factor, J., Ingalls, S., Kim, S.H., Ladner, R., Marks, K., Nelson, S., Pharaoh, A., Trimmer, R.,
18 Von Rosenberg, J., Wallace, G., and Weatherall, P.: Global Bathymetry and Elevation Data at
19 30 Arc Seconds Resolution: SRTM30_PLUS, *Mar. Geod.*, 32, 355-371, doi:
20 10.1080/01490410903297766, 2009.
- 21 Bidlot, J.-R.: Impact of ocean surface currents on the ECMWF forecasting system for
22 atmosphere circulation and ocean waves, GlobCurrent Preliminary User Consultation
23 Meeting, <http://globcurrent.ifremer.fr/component/k2/itemlist/category/118?Itemid=960>,
24 Brest, 7-9 March 2012.
- 25 Blanke, B. and Delecluse, P.: Variability of the tropical Atlantic-Ocean simulated by a
26 general-circulation model with 2 different mixed-layer physics, *J. Phys. Oceanogr.*, 23, 1363-
27 1388, 1993.
- 28 Brodeau, L., Barnier, B., Treguier, A.M., Penduff, T., and Gulev S.: An ERA40-based
29 atmospheric forcing for global ocean circulation models, *Ocean Modelling*, 31, issues 3-4, 88-
30 104, doi: 10.1016/j.ocemod.2009.10.005, 2010.



- 1 Bruinsma, S., Lemoine, J.-M., Biancale, R., and Vales, N.: CNES/GRGS 10-day gravity field
2 models (release 02) and their evaluation, *Adv. Space Res.*, 45, 4, 587-601, doi:
3 10.1016/j.asr.2009.10.012, 2010.
- 4 Chambers, D. P., Cazenave, A., Champollion, N., Dieng, H., Llovel, W., Forsberg, R., von
5 Schuckmann, K., and Wada, Y.: Evaluation of the global mean sea level budget between 1993
6 and 2014, *Surv. Geophys.*, 38, no. 1, 309-327, doi:10.1007/s10712-016-9381-3, 2017.
- 7 Chelton, D. B., Wentz, F. J., Gentemann, C. L., De Szoeko, R. A., and Schlax, M. G.:
8 Satellite microwave SST observations of transequatorial tropical instability waves, *Geophys.*
9 *Res. Lett.*, 27, 1239-1242, 2000.
- 10 Chen, J. L., Wilson, C. R., Tapley, B. D., Famiglietti, J. S., and Rodell, M.: Seasonal global
11 mean sea level change from satellite altimeter, GRACE, and geophysical models, *J. Geodesy*,
12 79, 532-539, doi:10.1007/s00190-005-0005-9, 2005.
- 13 Chevallier, M., G.C. Smith, J.-F. Lemieux, F. Dupont, G. Forget, Y. Fujii, F. Hernandez, R.
14 Msadek, K. A. Peterson, A. Storto, T. Toyoda, M. Valdivieso, G. Vernieres, H. Zuo, M.
15 Balmaseda, Y.-S. Chang, N. Ferry, G. Garric, K. Haines, S. Keeley, R. M. Kovach, T.
16 Kuragano, S. Masina, Y. Tang, H. Tsujino, X. Wang: Intercomparison of the Arctic sea ice
17 cover in global ocean-sea ice reanalyses from the ORA-IP project, *Clim. Dyn.*, 49: 1107,
18 <https://doi.org/10.1007/s00382-016-2985-y>, 2017.
- 19 Church, J. A., Clark, P. U., Cazenave, A., Gregory, J.-M., Jevrejeva, S., Levermann, A.,
20 Merrifield, M. A., Milne, G. A., Nerem, R. S., Nunn, P. D., Payne, A. J., Pfeffer, W. T.,
21 Stammer, D., and Unnikrishnan, A. S.: Sea Level Change. In: *Climate Change 2013: The*
22 *Physical Science Basis. Contribution of Working Group I to the Fifth Assessment Report of*
23 *the Intergovernmental Panel on Climate Change [Stocker, T.F., D. Qin, G.-K. Plattner, M.*
24 *Tignor, S.K. Allen, J. Boschung, A. Nauels, Y. Xia, V. Bex and P.M. Midgley (eds.)].*
25 *Cambridge University Press, Cambridge, United Kingdom and New York, NY, USA, 2013.*
- 26 Cravatte, S., Madec, G., Izumo, T., Menkes, C., and Bozec, A.: Progress in the 3D circulation
27 of the eastern equatorial Pacific in a climate, *Ocean Model.*, 17, 28-48, 2007.
- 28 Dai, A. and Trenberth, K. E.: Estimates of freshwater discharge from continents: latitudinal
29 and seasonal variations, *J. Hydrometeorol.*, 3, 660-687, 2002.
- 30 Dai A., Qian, T., Trenberth, K., and Milliman, J. D.: Changes in Continental Freshwater
31 Discharge from 1948 to 2004, *J. Climate*, vol. 22, p.2773-2792, 2009.



- 1 Dee, D. P., and Coauthors: The ERA-interim reanalysis: Configuration and performance of
2 the data assimilation system, *Quart. J. Roy. Meteor. Soc.*, 137, 553–597,
3 doi:<https://doi.org/10.1002/qj.828>, 2011.
- 4 Desroziers, G., Berre, L., Chapnik, B., and Polli, P.: Diagnosis of observation, background
5 and analysis-error statistics in observation space, *Q. J. R. Meteorol. Soc.*, 131, pp. 3385–3396,
6 doi: 10.1256/qj.05.108, 2005.
- 7 Drevillon, M., Greiner, E., Paradis, D., Payan, C., Lellouche, J.M., Reffray, G., Durand, E.,
8 Law-Chune, S., and Cailleau, S.: A strategy for producing refined currents in the Equatorial
9 Atlantic in the context of the search of the AF447 wreckage. *Ocean Dynamics*, 63, 63-82,
10 DOI 10.1007/s10236-012-0580-2, 2013.
- 11 Drillet, Y., Lellouche, J.-M., Levier, B., Drevillon, M., Le Galloudec, O., Reffray, G.,
12 Regnier, C., Greiner, E., and Clavier, M.: Forecasting the mixed layer depth in the north east
13 Atlantic: an ensemble approach, with uncertainties based on data from operational oceanic
14 systems *Ocean Sci. Discuss.*, 11, 1435-1472, [http://www.ocean-sci-](http://www.ocean-sci-discuss.net/11/1435/2014/osd-11-1435-2014.html)
15 [discuss.net/11/1435/2014/osd-11-1435-2014.html](http://www.ocean-sci-discuss.net/11/1435/2014/osd-11-1435-2014.html), 2014.
- 16 Estournel, C., Testor, P., Damien, P., D’ortenzio, F., Marsaleix, P., Conan, P., Kessouri, F.,
17 Durrieu de Madron, X., Coppola, L., Lellouche, J.-M., Belamari, S., Mortier, L., Ulses, C.,
18 Bouin, M.-N., and Prieur, L.: High resolution modeling of dense water formation in the north-
19 western Mediterranean during winter 2012-2013: Processes and budget, *J. Geophys. Res.*,
20 Wiley-Blackwell, 121 (7), pp.5367-5392, DOI:10.1002/2016JC011935, 2016.
- 21 Fichet, T. and Maqueda, M. A.: Sensitivity of a global sea ice model to the treatment of ice
22 thermodynamics and dynamics, *J. Geophys. Res.*, 102, 12609-12646, 1997.
- 23 Good, S.A., Martin, M.J., and Rayner, N.A.: EN4: quality controlled ocean temperature and
24 salinity profiles and monthly objective analyses with uncertainty estimates, *J. Geophys. Res.*,
25 118, 6704-6716, doi:10.1002/2013JC009067, 2013.
- 26 Grasso, L. D.: The differentiation between grid spacing and resolution and their application to
27 numerical modelling, *B. Am. Meteor. Soc.*, 81, 579-580, 2000.
- 28 Greiner, E., Benkiran, M., Blayo, E., and Dibarboure, G.: MERA-11 general scientific paper,
29 1992-2002 PSY1V2 reanalysis, reference MOO-MR-431-37-MER Mercator-Ocean,
30 Toulouse, France, 68 pp, 2006.



- 1 Grodsky, S. A., Lumpkin, R., and Carton, J. A.: Spurious trends in global surface drifter
2 currents, *Geophys. Res. Lett.*, 38, L10606, doi: 10.1029/2011GL047393, 2011.
- 3 Hilburn, K.: The passive microwave water cycle product, Remote Sensing Systems (REMSS)
4 Technical Report 072409, Santa Rosa (CA), 30 pp., 2009.
- 5 Hilburn, K., Smith D.K., and Mears C. A.: Annual Validation report: Rain, Remote Sensing
6 Systems, www.remss.com, 2014.
- 7 Hoaglin D., Mosteller F., and Tukey J. W.: Understanding Robust and Exploratory Data
8 Analysis, Wiley Series in probability and mathematical statistics, New-York, 1983.
- 9 Janowiak, J. E., Gruber, A., Kondragunta, C. R., Livezey, R.E., and Huffman G.J.: A
10 comparison of the NCEP-NCAR reanalysis precipitation and the GPCP rain gauge-satellite
11 combined dataset with observational error considerations, *J. of Climate*, vol. 11, 2960-2979,
12 1998.
- 13 Janowiak, J. E., Bauer, P., Wang, W., Arkin, P. A., and Gottschalck, J.: An evaluation of
14 precipitation forecasts from operational models and reanalysis including precipitations
15 variations associated with MJO activity, *Monthly weather Review*, 138, p. 4542-4560, 2010.
- 16 Juza, M., Moure, B., Lellouche, J.-M., Tonani, M., and Tintore, J.: From basin to sub-basin
17 scale assessment and intercomparison of numerical simulations in the Western Mediterranean
18 Sea, *Journal of Marine Systems*, 149, 36–49, <http://dx.doi.org/10.1016/j.jmarsys.2015.04.010>,
19 2015.
- 20 Gouretski, V. V. and Koltermann, K. P.: Woce global hydrographic climatology. Technical
21 Report 35/2004, Berichte des Bundesamtes fur Seeschifffahrt und Hydrographie, 2004.
- 22 Jackett, D. R. and McDougall, T. J.: Minimal Adjustment of Hydrographic Profiles to Achieve
23 Static Stability, *J. Atmos. Oceanic Technol.*, 12, 381–389, [https://doi.org/10.1175/1520-0426\(1995\)012<0381:MAOHPT>2.0.CO;2](https://doi.org/10.1175/1520-0426(1995)012<0381:MAOHPT>2.0.CO;2), 1995.
- 25 Kidd, C., Dawkins, E., and Huffman, G.: Comparison of Precipitation Derived from the
26 ECMWF Operational Forecast Model and Satellite Precipitation Datasets, *Journal of*
27 *Hydrometeorology*, 14 (5), p. 1463-1482, <https://doi.org/10.1175/JHM-D-12-0182.1>, 2013.
- 28 Kjerfve, B.: Tides of the Caribbean Sea, *J. Geophys. Res.*, 86(C5), 4243-4247,
29 doi:10.1029/JC086iC05p04243, 1981.

30



- 1 Koch-Larrouy, A., Madec, G., Blanke, B., and Molcard, R.: Water mass transformation along
2 the Indonesian throughflow in an OGCM, *Ocean Dynam.*, 58, 289-309, doi:10.1007/s10236-
3 008-0155-4, 2008.
- 4 Koenig, Z., Provost, C., Villaceros-Robineau, N., Sennechael, N., Meyer, A., Lellouche, J.-
5 M., and Garric, G.: Atlantic waters inflow north of Svalbard: Insights from IAOOS
6 observations and Mercator Ocean global operational system during N-ICE2015, *J. Geophys.*
7 *Res. Oceans*, 122, 1254–1273, doi:10.1002/2016JC012424, 2017.
- 8 Lagerloef, G., Schmitt, R., Schanze, J., and Kao, H. Y.: The Ocean and the global water cycle,
9 *Oceanography*, 23(4), 82-93, <http://dx.doi.org/10.5670/oceanog.2010.07>, 2010.
- 10 Large, W. G. and Yeager, S. G.: The global climatology of an interannually varying air–sea
11 flux data set, *Clim. Dynam.*, 33, 341-364, doi:10.1007/s00382-008-0441-3, 2009.
- 12 Lellouche, J.-M., Le Galloudec, O., Drevillon, M., Regnier, C., Greiner, E., Garric, G., Ferry,
13 N., Desportes, C., Testut, C.-E., Bricaud, C., Bourdalle-Badie, R., Tranchant, B., Benkiran,
14 M., Drillet, Y., Daudin, A., and De Nicola, C.: Evaluation of global monitoring and
15 forecasting systems at Mercator Ocean, *Ocean Sci.*, 9, 57-81, doi:10.5194/os-9-57-2013,
16 2013.
- 17 Lengaigne, M., Menkes, C., Aumont, O., Gorgues, T., Bopp, L., Andre, J.M., and Madec, G.:
18 Influence of the oceanic biology on the tropical Pacific climate in a coupled general
19 circulation model, *Clim. Dyn.*, 28, 503-507, DOI:10.1007/s00382-006-0200-2, 2007.
- 20 Levy, M., Estublier, A., and Madec, G.: Choice of an advection scheme for biogeochemical
21 models, *Geophys. Res. Lett.*, 28, 3725–3728, doi:10.1029/2001GL012947, 2001.
- 22 Locarnini, R. A., Mishonov, A. V., Antonov, J. I., Boyer, T. P., Garcia, H. E., Baranova, O.
23 K., Zweng, M. M., Paver, C. R., Reagan, J. R., Johnson, D. R., Hamilton, M., and Seidov,
24 D.: *World Ocean Atlas 2013, Volume 1: Temperature*. S. Levitus, Ed., A. Mishonov
25 Technical Ed.; NOAA Atlas NESDIS 73, 40 pp., 2013.
- 26 Madec, G. and Imbard M.: A global ocean mesh to overcome the North Pole singularity,
27 *Clim. Dynam.*, 12, 381-388, 1996.
- 28 Madec, G., and the NEMO team: NEMO ocean engine. Note du Pôle de modélisation, Institut
29 Pierre-Simon Laplace (IPSL), France, No. 27 ISSN, 1288-1619, 2008.
- 30 Menemenlis, D., Fukumori, I., and Lee, T.: Atlantic to Mediterranean Sea level difference
31 driven by winds near Gibraltar Strait, *J. Phys. Oceanogr.*, 37, 359–376, 2007.



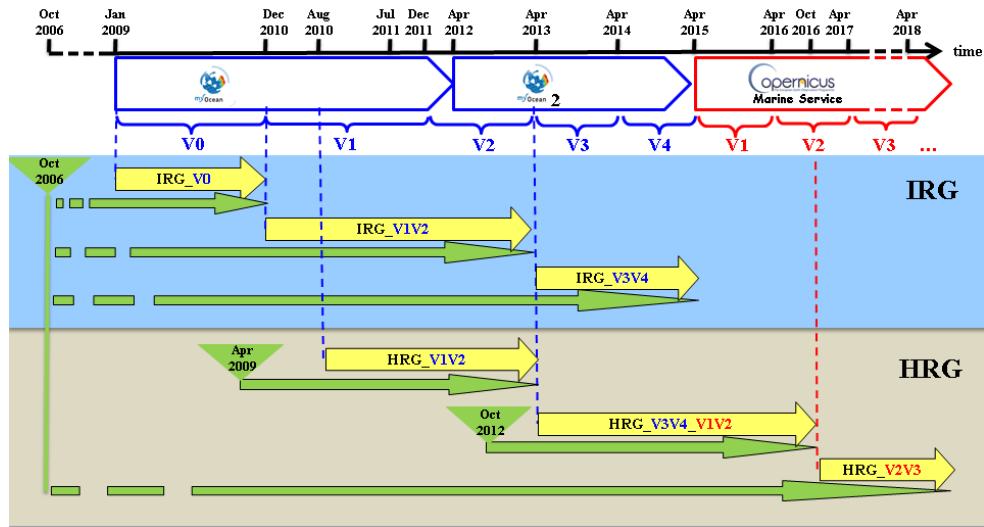
- 1 Pujol, M.-I., Faugère, Y., Taburet, G., Dupuy, S., Pelloquin, C., Ablain, M., and Picot, N.:
2 DUACS DT2014: the new multi-mission altimeter data set reprocessed over 20 years,
3 Ocean Sci., 12, 1067-1090, doi:10.5194/os-12-1067-2016, 2016.
- 4 Raynaud, L., Berre, L., and Desroziers, G.: Objective filtering of ensemble-based
5 background-error variances, Quarterly Journal of the Royal Meteorology Society, Vol. 135,
6 Issue 642, 1177–1199, 2009.
- 7 Renault, L., Molemaker, M. J., McWilliams, J. C., Shchepetkin, A. F., Lemarie, F., Chelton,
8 D., Illig, S., and Hall A.: Modulation of wind work by oceanic current interaction with the
9 atmosphere, Journal of Physical Oceanography, 46 (6), 1685-1704, ISSN 0022-3670, 2016.
- 10 Rio, M. H., Guinehut, S., and Larnicol, G.: New CNES-CLS09 global mean dynamic
11 topography computed from the combination of GRACE data, altimetry, and in situ
12 measurements, J. Geophys. Res., 116, C07018, doi:10.1029/2010JC006505, 2011.
- 13 Rio, M.H.: Use of altimeter and wind data to detect the anomalous loss of SVP-type drifter's
14 drogue, Journal of Atmospheric and Oceanic Technology, DOI:10.1175/JTECH-D-12-
15 00008.1, 2012.
- 16 Rio, M.-H., Mulet, S., and Picot, N.: Beyond GOCE for the ocean circulation estimate:
17 Synergetic use of altimetry, gravimetry, and in situ data provides new insight into geostrophic
18 and Ekman currents, Geophys. Res. Lett., 41, doi:10.1002/2014GL061773, 2014.
- 19 Roemmich, D. and Gilson, J.: The 2004–2008 mean and annual cycle of temperature, salinity,
20 and steric height in the global ocean from the Argo Program, Progress in Oceanography,
21 Volume 82, Issue 2, 81–100, <https://doi.org/10.1016/j.pocean.2009.03.004>, 2009.
- 22 Roquet, F., Charrassin, J. B., Marchand, S., Boehme, L., Fedak, M., Reverdin, G., and Guinet,
23 C.: Delayed-mode calibration of hydrographic data obtained from animal-borne satellite relay
24 data loggers, J. Atmos. Ocean. Tech., 28, 787–801, 2011.
- 25 Roulet, G. and Madec, G.: Salt conservation, free surface, and varying levels: a new
26 formulation for ocean general circulation models, J. Geophys. Res., 105, 23927–23942, 2000.
- 27 Schweiger, A., Lindsay, R., Zhang, J., Steele, M., and Stern, H.: Uncertainty in modeled
28 arctic sea ice volume, J. Geophys. Res., doi:10.1029/2011JC007084, 2011.
- 29 Scott, R., Ferry, N., Drevillon, M., Barron, C.N., Jourdain, N.C., Lellouche, J.-M., Metzger,
30 E. J., Rio, M. H., and Smedstad, O. M.: Estimates of surface drifter trajectories in the



- 1 Equatorial Atlantic: a multi-model ensemble approach. *Ocean Dynamics*, 62, 1091-1109. doi
2 10.1007/s10236-012-0548-2, 2012.
- 3 Silva, T. A. M., Bigg, G. R., and Nicholls, K. W.: Contribution of giant icebergs to the
4 Southern Ocean freshwater flux, *J. Geophys. Res.*, 111, C03004, doi:10.1029/2004JC002843,
5 2006.
- 6 Smith, G.C., Roy, F., Reszka, M., Surcel Colan, D., He, Z., Deacu, D., Belanger, J.-M.,
7 Skachko, S., Liu, Y., Dupont, F., Lemieux, J-F., Beaudoin, C., Tranchant, B., Drevillon, M.,
8 Garric, G., Testut, C.-E., Lellouche, J.-M., Pellerin, P., Ritchie, H., Lu, Y., Davidson, F.,
9 Buehner, M., Caya, A., and Lajoie, M.: Sea ice forecast verification in the Canadian Global
10 Ice Ocean Prediction System, *Quarterly Journal of the Royal Meteorology Society*, Vol.142,
11 Issue 695, Pages 659–671, 2016.
- 12 Song, Y. T.: Estimation of interbasin transport using ocean bottom pressure: Theory and
13 model for Asian marginal seas, *J. Geophys. Res.*, 111, C11S19, doi:10.1029/2005JC003189,
14 2006.
- 15 Storto, A., Russo, I., and Masina, S.: Interannual response of global ocean hindcasts to a
16 satellite-based correction of precipitation fluxes, *Ocean Sci. Discuss.*,
17 <https://doi.org/10.5194/osd-9-611-2012>, 2012.
- 18 Szekely, T., Gourrion, J., Pouliquen, S., and Reverdin, G.: CORA, Coriolis Ocean Dataset for
19 Reanalysis. SEANOE doi:<http://doi.org/10.17882/46219>, 2016.
- 20 Talagrand, O.: A posteriori evaluation and verification of analysis and assimilation
21 algorithms, *Proc. of ECMWF Workshop on Diagnosis of Data Assimilation System*
22 (Reading), 17–28, 1998.
- 23 Tranchant, B., Reffray, G., Greiner, E., Nugroho, D., Koch-Larrouy, A., and Gaspar, P.:
24 Evaluation of an operational ocean model configuration at 1/12° spatial resolution for the
25 Indonesian seas (NEMO2.3/INDO12) – Part 1: Ocean physics, *Geosci. Model Dev.*, 9, 1037-
26 1064, 2016.
- 27 Troccoli, A. and P. Kallberg, P.: Precipitation correction in the ERA-40 reanalysis, ERA-40
28 Project Report Series N°13, 1-10, 2004.
- 29 Vinogradov, S.V. and Ponte R.M.: Low frequency variability in coastal sea level from tide
30 gauges and altimetry, *J. Geophys. Res.*, 116, C07006, doi:10/1029/2011JC007034, 2011.



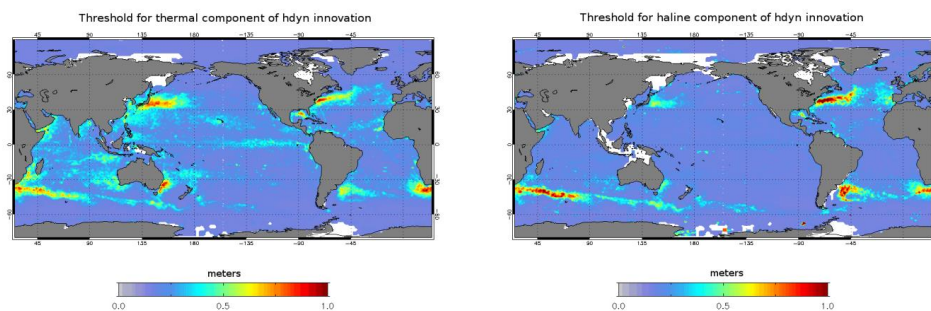
- 1 Willebrand, J. , Barnier, B. , Böning, C. , Dieterich, C. , Killworth, P. D. , Le Provost, C. , Jia,
2 Y., Molines, J. M., and New, A. L.: Circulation characteristics in three eddy-permitting
3 models of the North Atlantic, *Progress in Oceanography*, 48(2), pp. 123-161, 2001.
- 4 Williams, J. and Hughes, C.W.: The coherence of small island sea level with the wider ocean:
5 a model study, *Ocean Sci.*, 9, 111-119, 2013.
- 6 Zweng, M. M., Reagan, J. R., Antonov, J. I., Locarnini, R. A., Mishonov, A., Boyer, T. P.,
7 Garcia, H. E., Baranova, O. K., Paver, C. R., Johnson, D. R., Seidov, D., and Biddle, M.:
8 *World Ocean Atlas 2013, Volume 2: Salinity*. S. Levitus, Ed., A. Mishonov, Technical
9 Ed.; NOAA Atlas NESDIS 74, 40 pp., 2013.
- 10 Zygmontowska, M., Rampal, P., Ivanova, N., and Smedsrud, L. H.: Uncertainties in Arctic sea
11 ice thickness and volume: new estimates and implications for trends, *The Cryosphere*, 8, 705-
12 720, <https://doi.org/10.5194/tc-8-705-2014>, 2014.



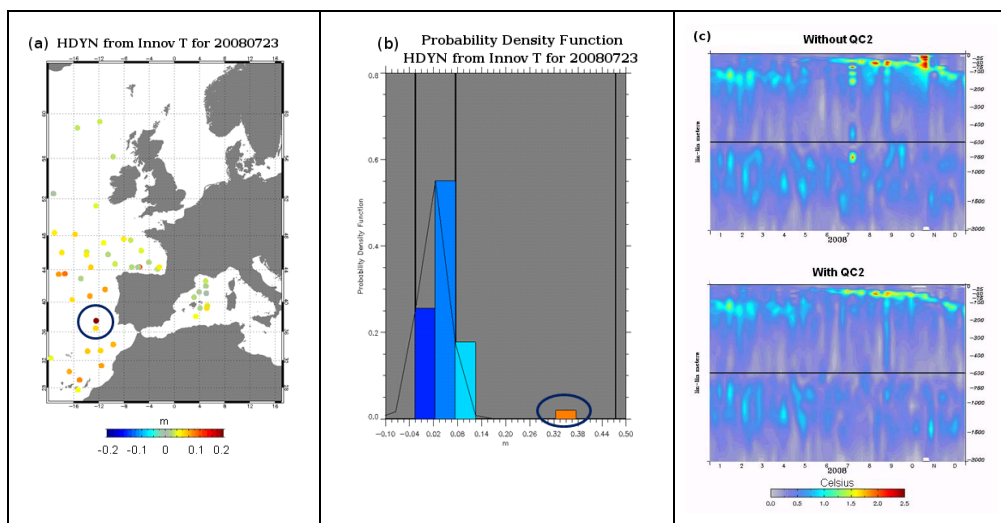
1

2 **Figure 1:** Timeline of the Mercator Ocean global analysis and forecasting systems for the various milestones
 3 (from V0 to V4) of past MyOcean project and for milestones V1, V2, V3 of the current CMEMS. Real-time
 4 productions are in yellow. Available Mercator Ocean simulations are in green including the catch-up to real-
 5 time. Global Intermediate Resolution (respectively High Resolution) system at $1/4^\circ$ (respectively $1/12^\circ$) is
 6 referred to as IRG (respectively HRG). Milestones are written in blue for MyOcean project and in red for
 7 CMEMS.

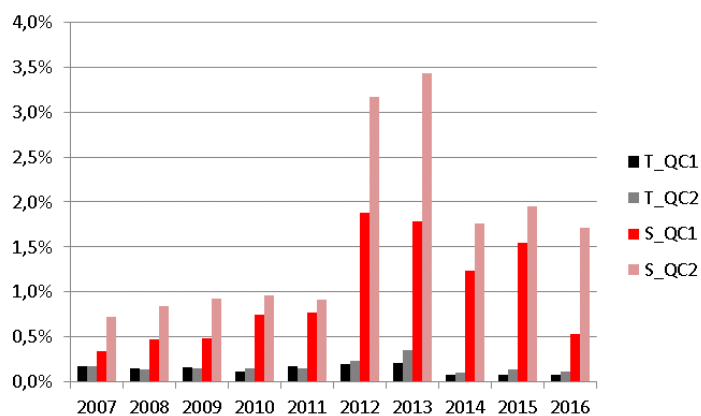
8



1 **Figure 2:** Thresholds used for QC2 for thermal component of dynamical height innovation (left
2 panel: $threshold_T$) and for haline component of dynamical height innovation (right panel: $threshold_S$). Units
3 are meters.
4

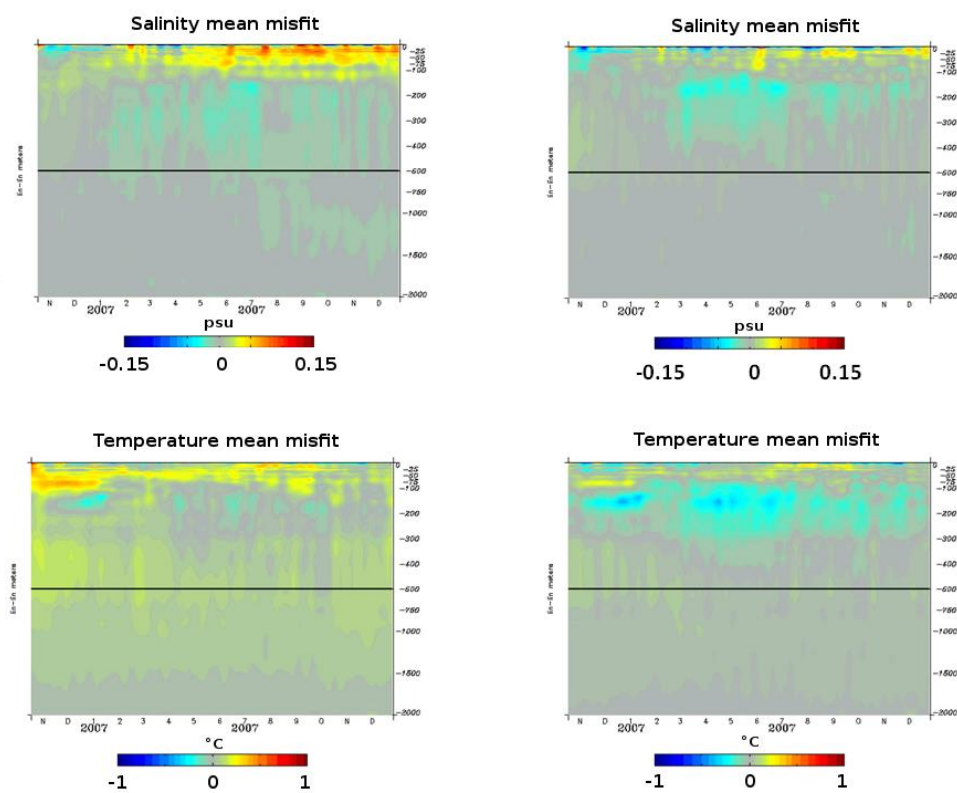


1 **Figure 3:** Statistics in the Azores region: a) absolute value of dynamical height innovations (in meters) from
2 temperature innovations for the 7-day assimilation cycle from 16 July 2008 to 23 July 2008, b) PDF of these
3 dynamical height innovations (the value 0.3 m appears in the tail of the PDF), c) RMS innovation with respect to
4 the vertical temperature profiles over the year 2008 for two “twins” simulations (without and with QC2). These
5 last scores are averaged over all seven days of the data assimilation window, with a lead time equal to 3.5 days.
6 Units are °C.

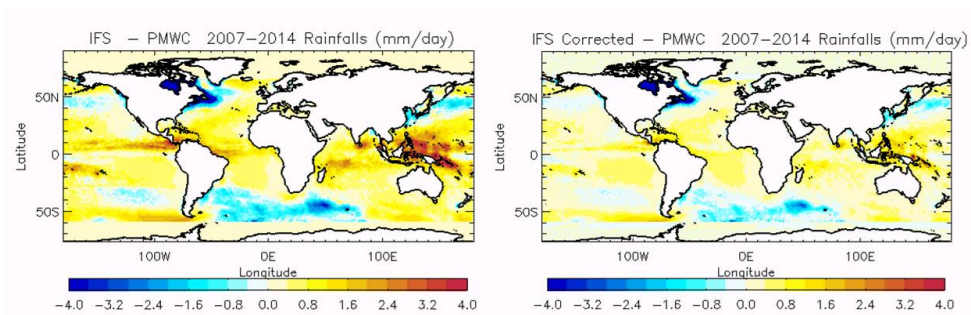


1

2 **Figure 4:** Statistics of suspicious temperature (T) and salinity (S) detected by QC1 (T_QC1 and S_QC1) and by
3 QC2 (T_QC2 and S_QC2) quality controls as a function of year in the PSY4V3 2007-2016 simulation time
4 period.



1
2 **Figure 5:** Diagnostics (time series) with respect to the vertical temperature and salinity profiles over the October
3 2006 - December 2007 period. Mean misfit between observations and model for salinity (top panels, units in
4 psu) and for temperature (low panels, units in °C), starting from WOA09 climatology (left panels) and robust
5 EN4 (right panels).

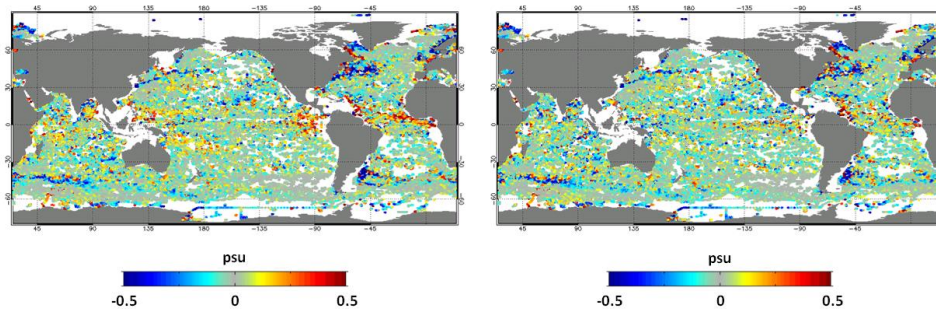


1

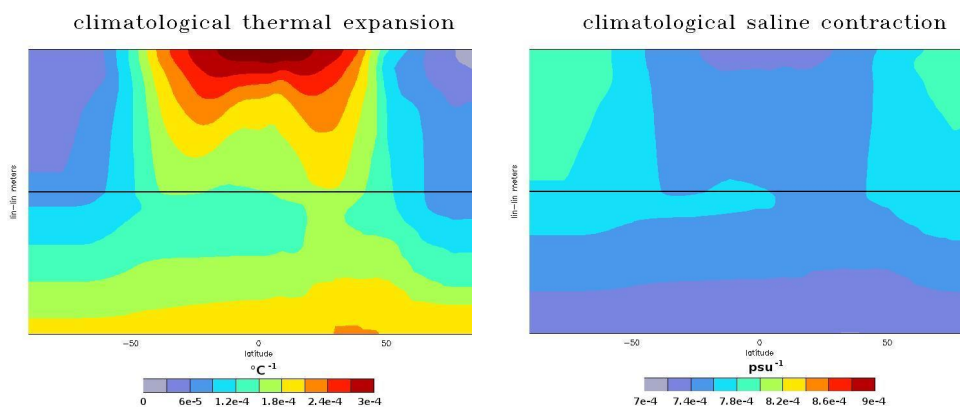
2 **Figure 6:** Mean 2007-2014 IFS ECMWF atmospheric precipitation bias (units in mm day^{-1}) with respect to
3 PMWC product without (left map) and with (right map) correction.



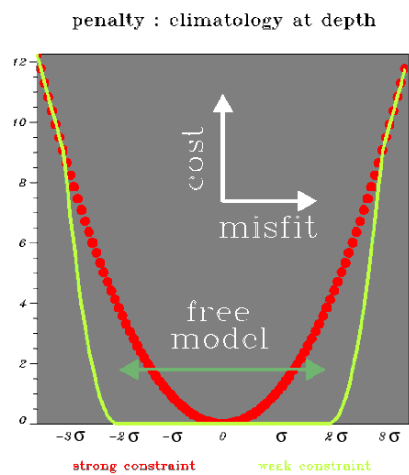
Mean surface salinity innovation (2011)



1
2 **Figure 7:** Mean surface salinity innovation (difference between the assimilated observation and the model, units
3 in psu) on the year 2011. On the left, the innovation resulting from the use of the original IFS field, and on the
4 right, the innovation resulting from the use of the corrected IFS field.

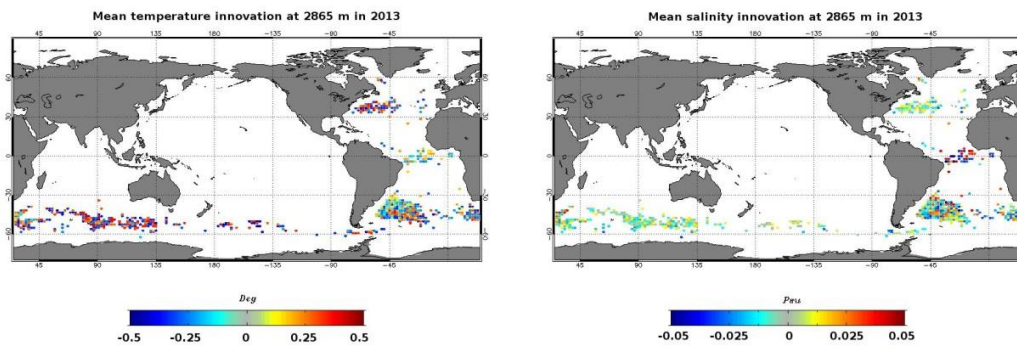


1 **Figure 8:** Climatological thermal expansion ($^{\circ}\text{C}^{-1}$) and saline contraction (psu^{-1}) as a function of the latitude and
2 the depth.

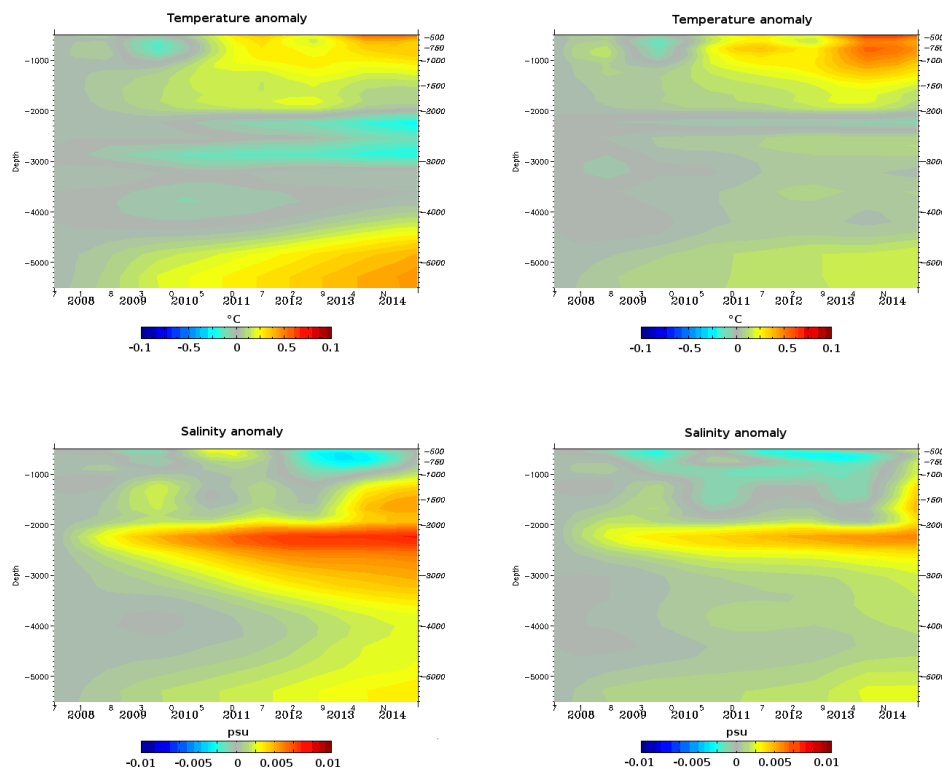


1

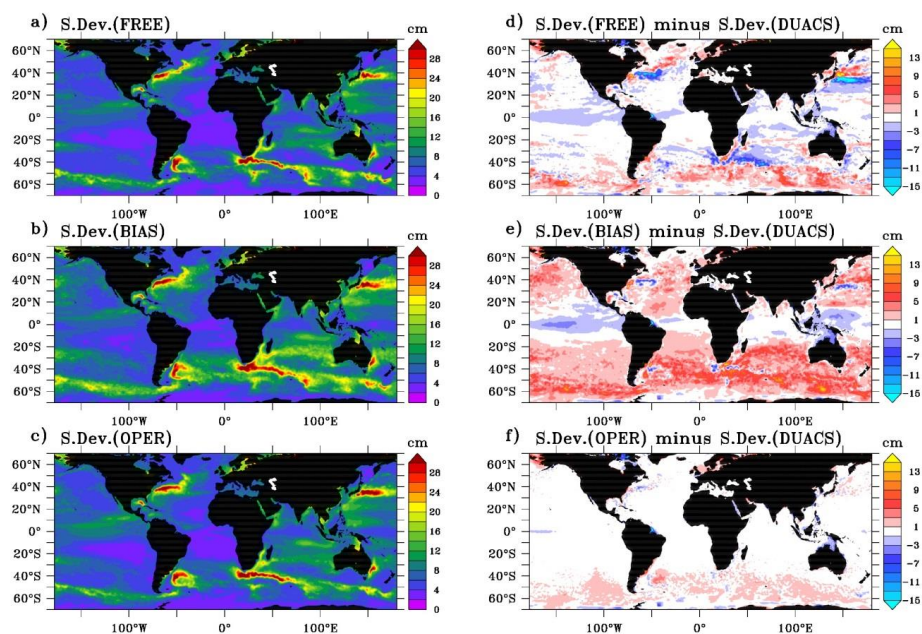
2 **Figure 9:** Non-Gaussian error for climatology (corresponding to a weak constrain of the system in green). A cost
3 equal to zero corresponds to an infinite observation error, namely a system operation in a free mode (without
4 assimilation of climatology).



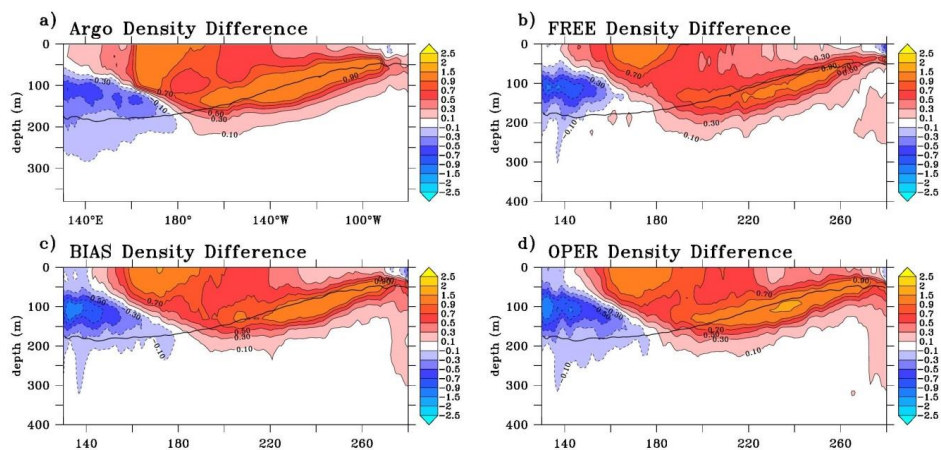
1 **Figure 10:** Mean temperature (on the left, units in °C) and salinity (on the right, units in psu) innovations in
2 2013 at 2865 m for the system PSY4V3.



1 **Figure 11** : Temperature (top panels, units in °C) and salinity (low panels, units in psu) annual anomalies over
2 depth (500-5000m) and time (2007-2014) for latitudes between 30° S and 60° S. The simulation on the left does
3 not assimilate climatological vertical profiles while the simulation on the right assimilates them. Annual anomaly
4 for a specific year is computed as the difference between the annual mean of this year and the annual mean of the
5 year 2007.

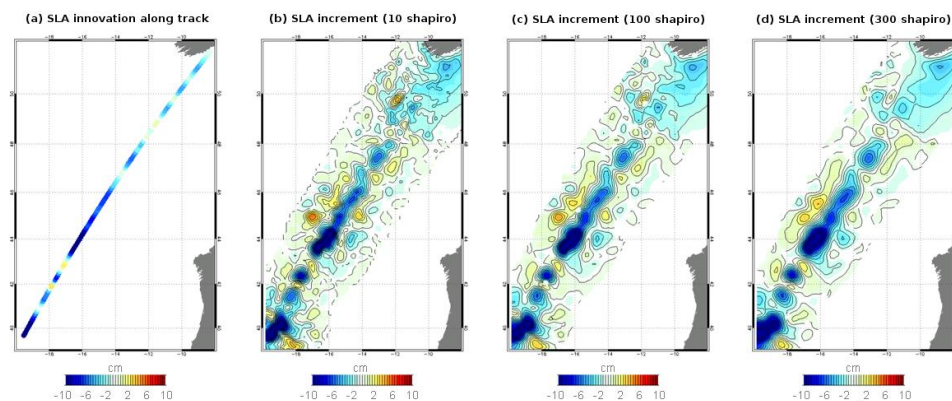


1
2 **Figure 12:** 2007-2015 SSH standard deviation (diagnostics made with 1 point every 3 horizontally and 1 day
3 every 5) of the 1/12° PSY4 simulations (a,b,c) and difference of SSH model standard deviation with the one of
4 DUACS product (d,e,f). Units are cm.

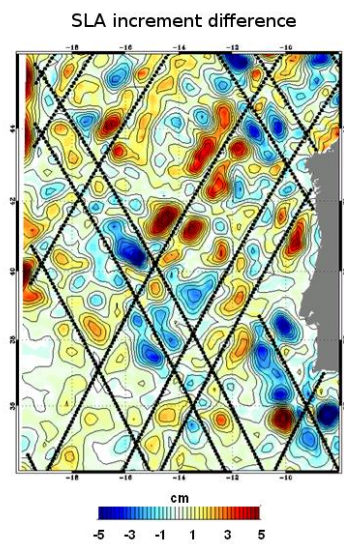


1

2 **Figure 13:** Density difference “OCT-DEC 2008 minus OCT-DEC 2009” in the equatorial Pacific (2° S-2° N)
3 above 400 m depth (a-d) from the SCRIPPS Argo product (a), and the three 1/12° PSY4 FREE, BIAS and OPER
4 simulations (b-d). The black line indicates the 2007-2015 Argo mean position of the pycnocline depth (isopycn
5 1025 kg m⁻³).

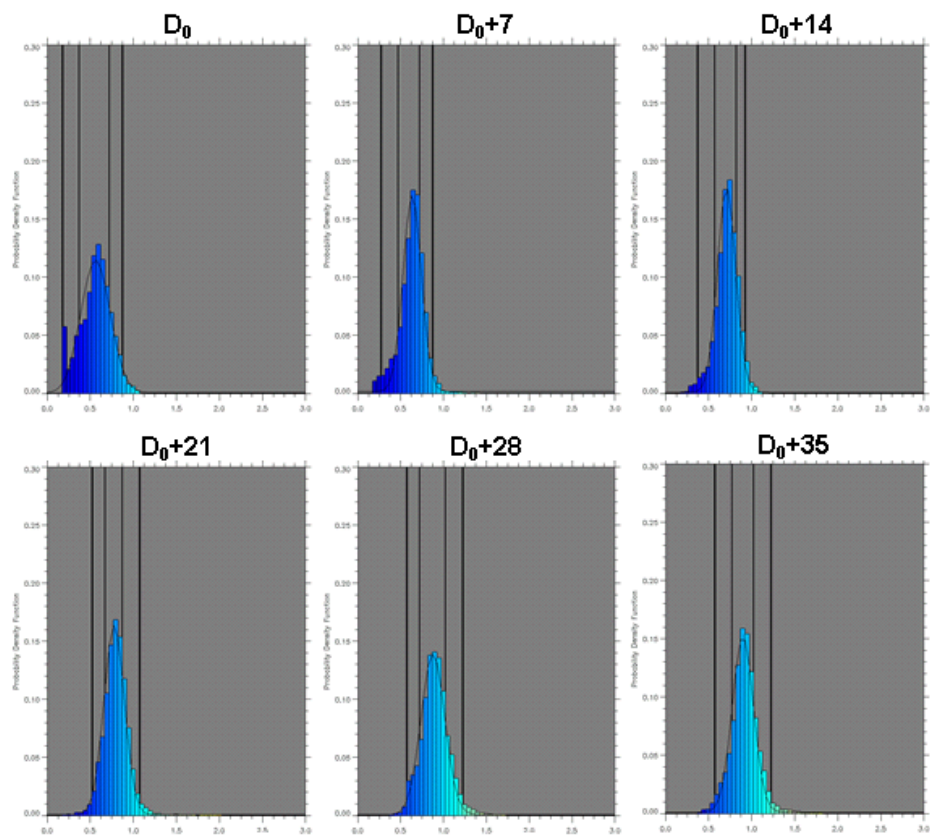


1
2 **Figure 14:** SLA innovation along a single assimilated track altimeter (a). SLA increments respectively with 10
3 (b), 100 (c) and 300 (d) Shapiro passes as anomaly filtering. These experiments have been performed with a
4 system at $1/12^\circ$. Unit is cm.



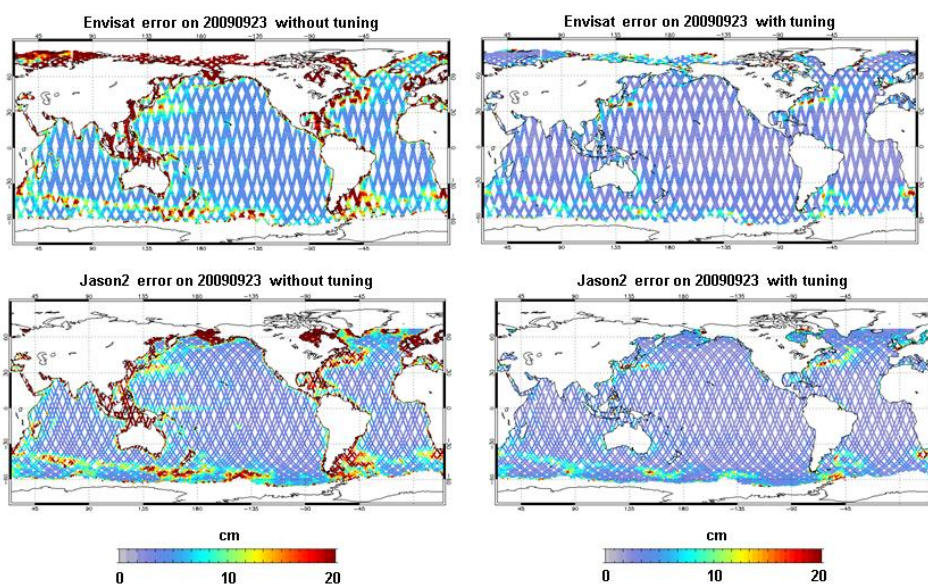
1

2 **Figure 15:** SLA increment difference using 10 and 300 Shapiro passes as anomaly filtering. The black lines
3 represent the position of the assimilated altimeter tracks. Unit is cm.



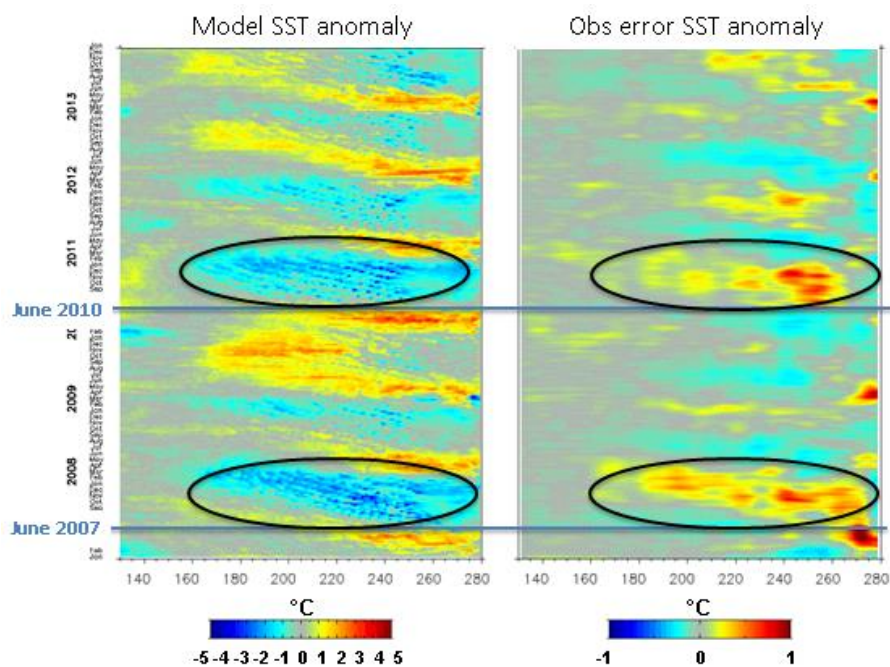
1

2 **Figure 16:** Evolution of the PDF of the ratio for Envisat satellite from D_0 to D_0+35 days. D_0 corresponds to the
3 first day where Envisat is assimilated by the system.



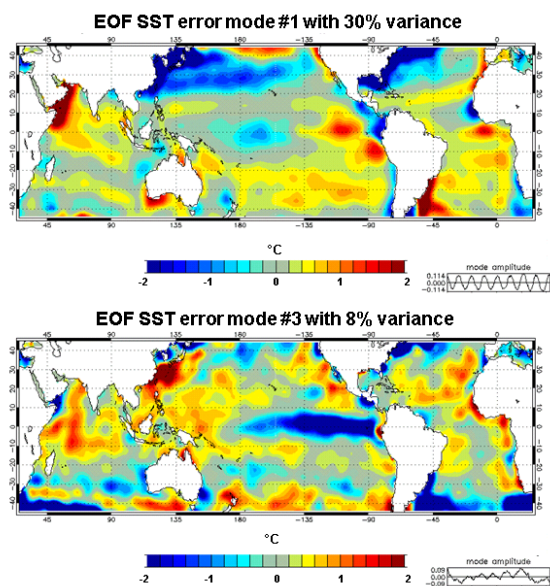
1

2 **Figure 17:** Envisat (top panels) and Jason2 (low panels) satellite observation errors used on the 7-day
3 assimilation cycle ending September, 23, 2009 without tuning (left panels) and with tuning
4 method. Unit is cm.



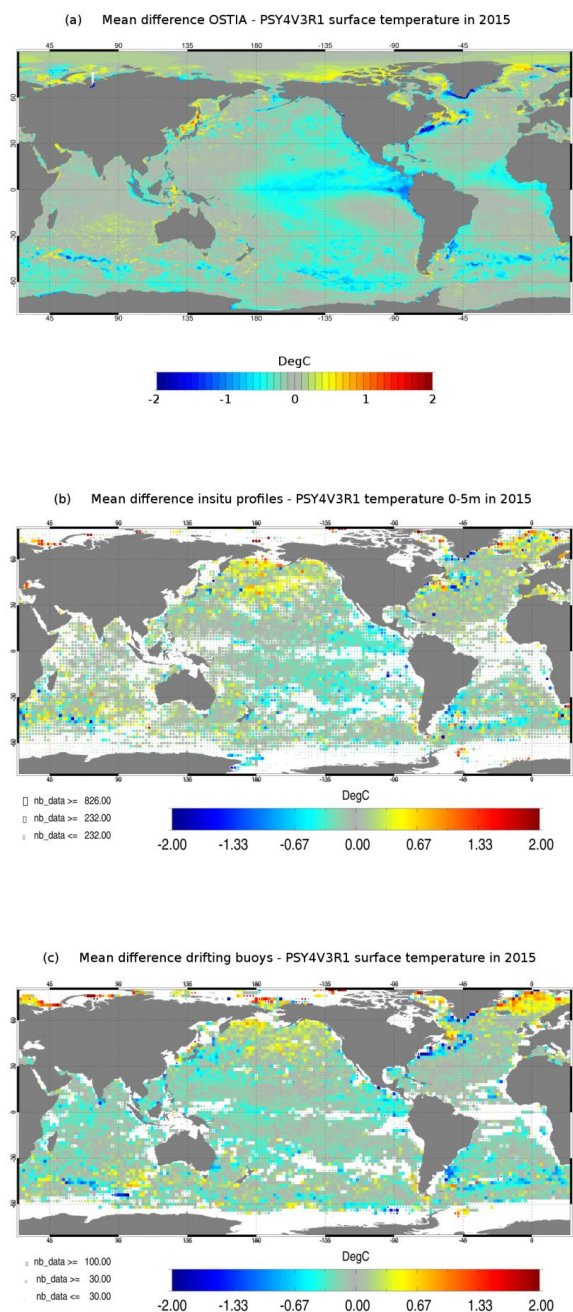
1

2 **Figure 18:** Evolution in time of model SST anomaly (on the left) and SST observation error anomaly tuned by
3 “Desroziers” method (on the right) for a section at 3° N. The blue lines represent the beginning of La Niña
4 episodes (mid-2007 and mid-2010). The black ellipses highlight periods when TIWs are more marked. Units are
5 °C.

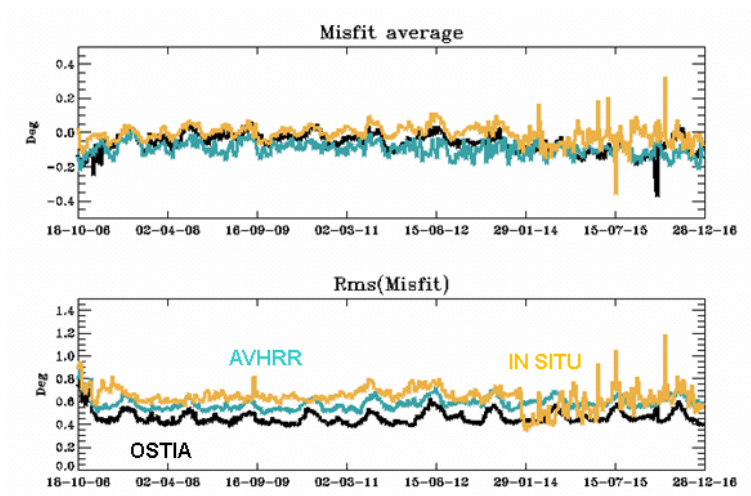


1

2 **Figure 19:** 1st EOF (top panel) and 3th EOF (bottom panel) of sea surface temperature observation error (°C)
3 over the 2007-2015 time period. The time series at the bottom of each panel correspond to the mode amplitude.



1 **Figure 20:** Mean SST residuals (units in °C) over the year 2015: OSTIA SST minus PSY4V3 (a), in situ SST
2 minus PSY4V3 (b) and drifting buoys SST minus PSY4V3 (c).

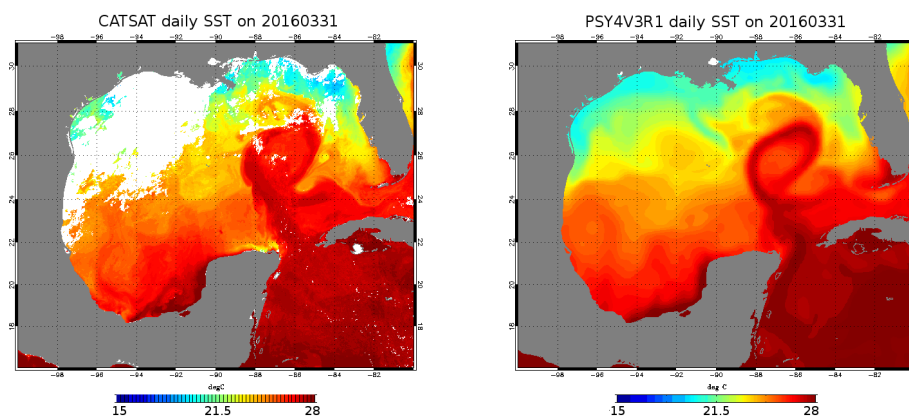


1

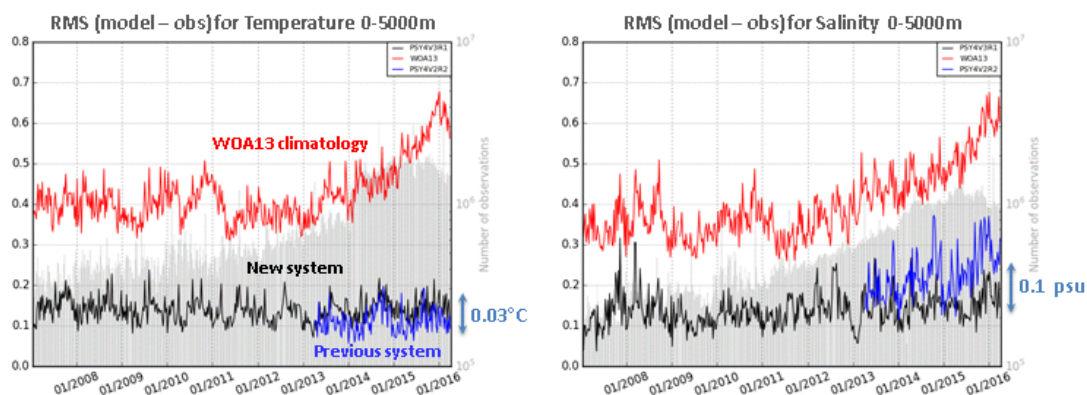
2 **Figure 21:** Time series of SST (units in °C) global misfit average (top) and RMS (bottom) for OSTIA
3 observations (black line, assimilated), NOAA AVHRR observations (blue line, not assimilated), and in situ
4 observations (orange line, assimilated), from October 2006 to December 2016.



1



2 **Figure 22:** High resolution CATSAT SST from CLS (on the left) and PSY4V3 SST (on the right) on March 31,
3 2016. Unit is °C.

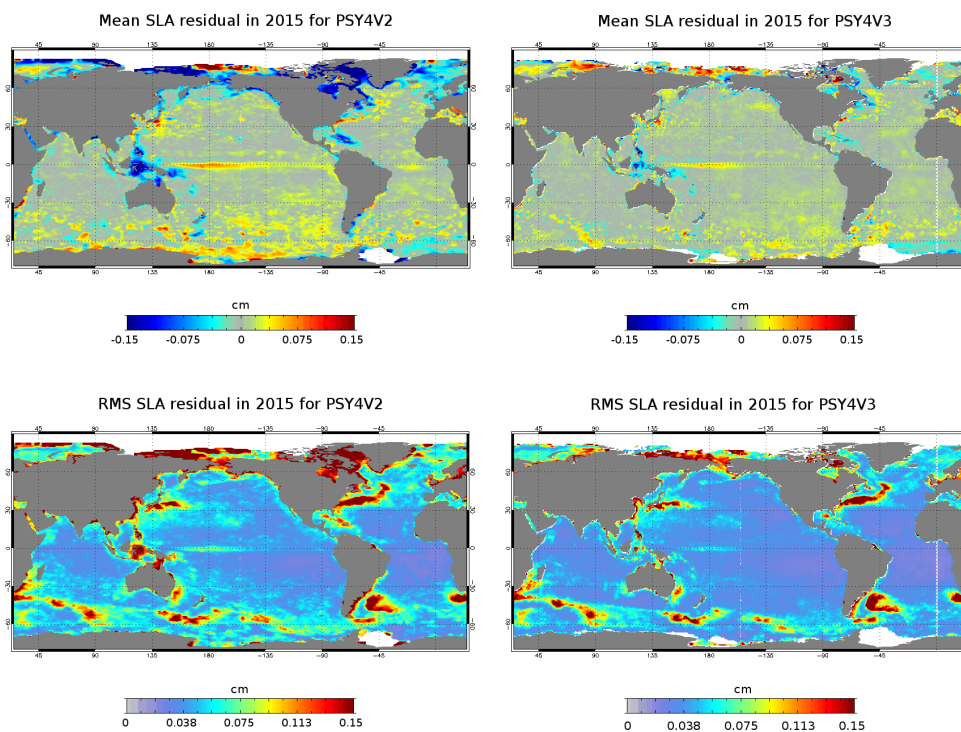


1

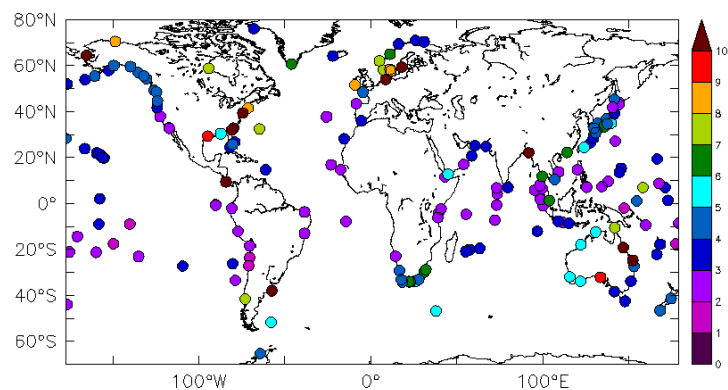
2 **Figure 23:** Time series of the 0-5000m RMS difference between the model analysis and the in situ observations
3 for previous system PSY4V2 (in blue), new system PSY4V3 (in black) and the WOA13v2 climatology (in red).
4 Left panel: temperature (unit in °C), right panel: salinity (unit in psu). Time series of the number of available
5 observations appear in grey.



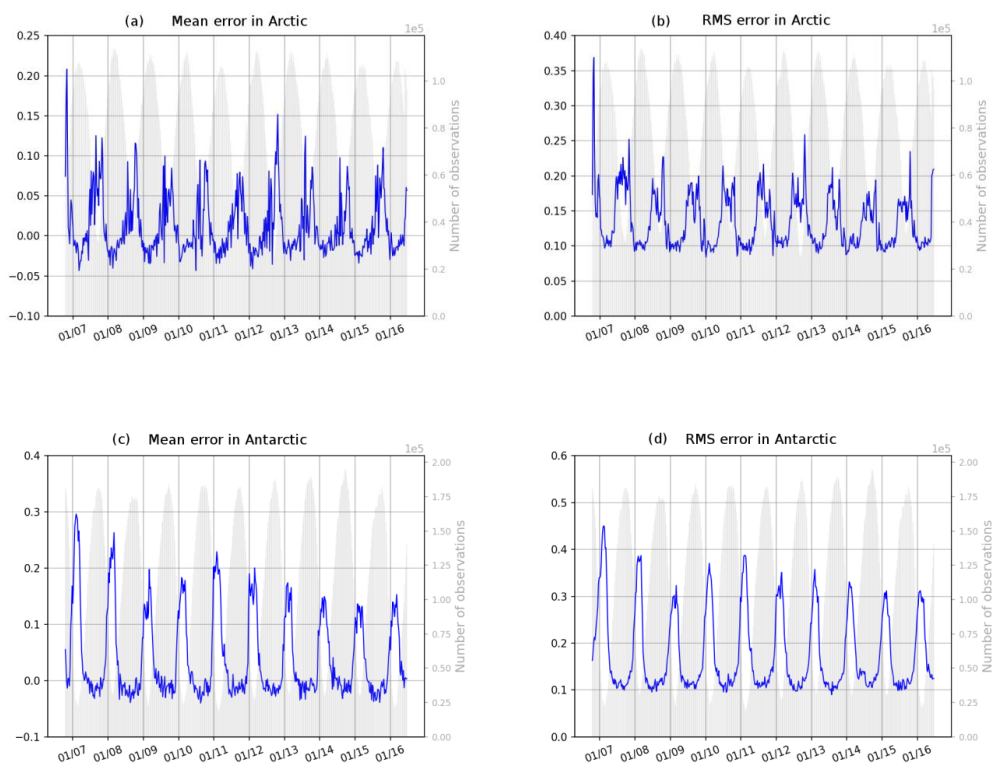
1



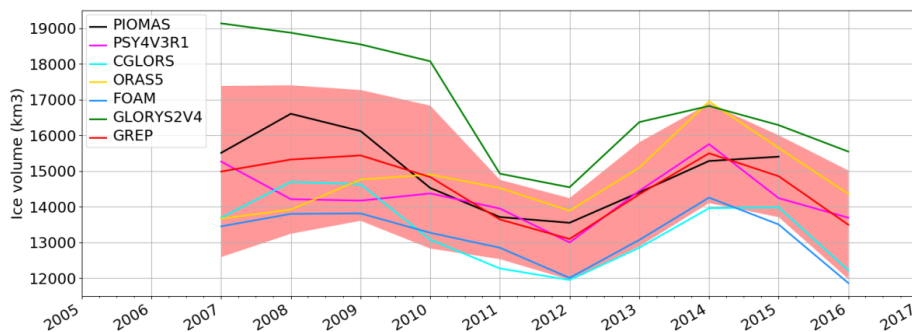
2 **Figure 24:** Mean residual errors (top panels) and RMS residual errors (low panels) of SLA in 2015, for the
3 previous system PSY4V2 (on the left) and the new system PSY4V3 (on the right). Unit is cm.



1
2 **Figure 25:** Sea surface height RMS difference between tide gauges observations and the system PSY4V3 for the
3 year 2015. Unit is cm.

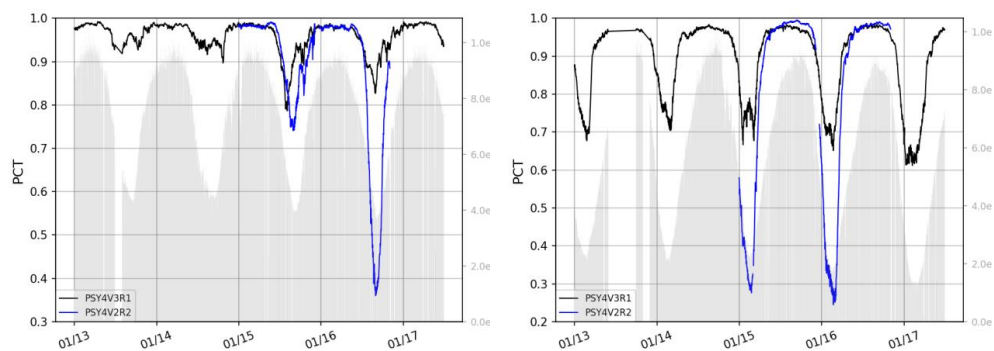


1 **Figure 26:** Time series of (observation-forecast) mean (a and c) and RMS (b and d) differences of sea ice
2 concentration (0 means no ice, 1 means 100 % ice cover) in the Arctic Ocean (a and b) and Antarctic Ocean (c
3 and d). The assimilated observations are the sea ice concentrations from OSI TAC. Time series of the number of
4 available observations appear in grey.

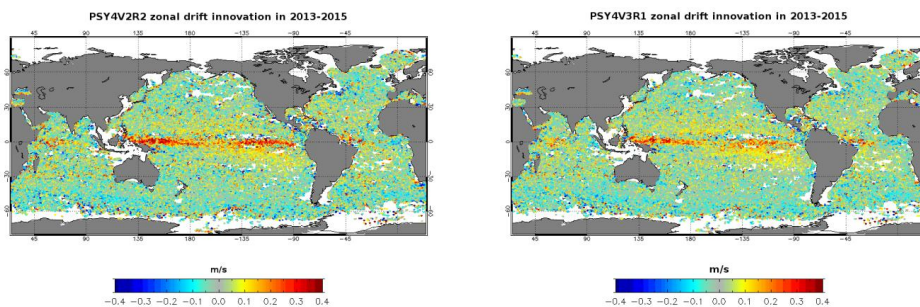


1

2 **Figure 27:** Time series over the 2007-2016 period of the sea ice volume in Arctic for several systems: GREP
3 composed by the four members GLORYS2V4 from Mercator Ocean (France), ORAS5 from ECMWF,
4 FOAM/GloSea from Met Office (UK) and C-GLORS from CMCC (Italy); PSY4V3 from Mercator Ocean
5 (France); PIOMAS product. The spread of GREP product is represented in light red. Unit is km^3 .



1 **Figure 28:** Time series of the PCT quantity for PSY4V2 (in blue) and PSY4V3 (in black). The left panel
2 corresponds to Arctic and the right panel to Antarctic. Time series of the number of available observations
3 appear in grey.



1 **Figure 29:** Mean zonal drift innovation (m s^{-1}) with PSY4V2 (on the left) and PSY4V3 (on the right) over the
2 time period 2013-2015. Observations come from Argo surface floats and a surface drifters corrected dataset
3 (Rio, 2012). Units are m s^{-1} .
4



System acronym	Domain	Resolution	Model	Assimilation	Assimilated observations	MyOcean version	Mercator system reference
IRG_V0	global	Horizontal: 1/4° Vertical: 50 levels	ORCA025 NEMO 1.09 LIM2, Bulk CLIO 24 h atmospheric forcing	SAM (SEEK)	"RTG" SST SLA T/S vertical profiles	V0	PSY3V2R1
IRG_V1V2	global	Horizontal: 1/4° Vertical: 50 levels	ORCA025 NEMO 3.1 LIM2 EVP, Bulk CORE 3 h atmospheric forcing	SAM (SEEK) IAU 3D-VAR bias correction	"RTG" SST SLA T/S vertical profiles	V1/V2	PSY3V3R1
IRG_V3V4	global	Horizontal: 1/4° Vertical: 50 levels	ORCA025 NEMO 3.1 LIM2 EVP, Bulk CORE 3 h atmospheric forcing New parameterization of vertical mixing Taking into account ocean colour for depth of light extinction Large scale correction to the downward radiative and precipitation fluxes Adding runoff for iceberg melting Adding seasonal cycle for surface mass budget	SAM (SEEK) IAU 3D-VAR bias correction Obs. errors higher near the coast (for SST and SLA) and on shelves (for SLA) MDT error adjusted Increase of Envisat altimeter error QC on T/S profiles New correlation radii	"AVHRR+AMSRE" SST SLA T/S vertical profiles MDT "CNES-CLS09" adjusted Sea Mammals T/S vertical profiles		PSY3V3R3

1 **Table 1:** Specifics of the Mercator Ocean IRG systems. In bold, the major upgrades with respect to the previous version. Available and operational production periods are
 2 described in Fig. 1.



System acronym	Domain	Resolution	Model	Assimilation	Assimilated observations	MyOcean CMEMS version	Mercator system reference
HRG_V1V2	global	Horizontal: 1/12° Vertical: 50 levels	ORCA12 NEMO 1.09 LIM2, Bulk CLIO 24 h atmospheric forcing	SAM (SEEK) IAU	"RTC" SST SLA T/S vertical profiles	V1/V2	PSY4V1R3
HRG_V3V4_V1V2	global	Horizontal: 1/12° Vertical: 50 levels	ORCA12 NEMO 3.1 LIM2 EVP, Bulk CORE 3 h atmospheric forcing New parameterization of vertical mixing Taking into account ocean color for depth of light extinction Large scale correction to the downward radiative and precipitation fluxes Adding runoff for iceberg melting Adding seasonal cycle for surface mass budget	SAM (SEEK) IAU 3D-VAR bias correction Obs. errors higher near the coast (for SST and SLA) and on shelves (for SLA) MDT error adjusted Increase of Envisat altimeter error QC on T/S profiles New correlation radii	"AVHRR+AMSRE" SST SLA T/S vertical profiles	V3/V4 V1/V2	PSY4V2R2
HRG_V2V3	global	Horizontal: 1/12° Vertical: 50 levels	ORCA12 NEMO 3.1 LIM2 EVP, Bulk CORE 3 h atmospheric forcing New parameterization of vertical mixing Taking into account ocean colour for depth of light extinction Adding seasonal cycle for surface mass budget 50 % of model surface currents used for surface momentum fluxes Updated runoff from Dai et al., 2009 + runoff fluxes coming from Greenland and Antarctica Addition of a trend (2.2mm yr ⁻¹) to the runoff Global steric effect added to the sea level New correction of precipitations using satellite data + no more correction of the downward radiative fluxes Correction of the concentration/dilution water flux term Relaxation toward WOA13v2 at Gibraltar and Bab-el-Mandeb	SAM (SEEK) IAU 3D-VAR bias correction (1 month time window) MDT error adjusted Increase of Envisat altimeter error QC on T/S profiles New correlation radii Addition of a second QC on T/S vertical profiles Adaptive tuning of observation errors for SLA and SST New 3D observation errors files for assimilation of in situ profiles Use of the SSH increment instead of the sum of barotropic and dynamic height increments Global mean increment of the total SSH is set to zero	CMEMS OSTIA SST SLA T/S vertical profiles MDT adjusted based on CNES-CLS13 Sea Mammals T/S vertical profiles CMEMS Sea Ice Concentration WOA13v2 climatology (temperature and salinity) constrain below 2000m (assimilation using a non-Gaussian error at depth)	V2/V3	PSY4V3R1

Table 2: Specifics of the Mercator Ocean HRG systems. In bold, the major upgrades with respect to the previous version. Available and operational production periods are described in Fig. 1.



	AMSR Ice	AMSR Water
Model Ice	Hit ice	False Alarm
Model Water	Miss	Hit water

1 **Table 3:** Contingency table entries for sea ice verification of PSY4V3 system as compared to AMSR sea ice
2 concentration observations.

3